Chapter 6
Interactions

Abstract In quantum mechanics the observable phenomena are interactions, expressed as matrix elements of operators in a function space. These spaces and operators are like communicating vessels, reality is neither the operation nor the representation, but the interaction. The evaluation of the corresponding matrix elements requires the coupling of representations, and can be factorized into an intrinsic scalar quantity that contains the physics of the interaction, and a tensorial coupling coefficient that contains its symmetry. This factorization is first illustrated for the case of overlap integrals, where the operator is just the unit operator, and then extended to the case of non-trivial operators, such as the Hamiltonian, and electric and magnetic dipole operators. The Wigner–Eckart theorem is introduced, together with the symmetry selection rules, both at the level of representations and subrepresentations. The results are applied to chemical reaction theory, and to the theory of the Jahn–Teller effect. Selection rules are illustrated for linear and circular dichroism. Finally, the polyhedral Euler theorem is introduced and applied to valence-bond theory for clusters.

Contents

A.J. Ceulemans, *Group Theory Applied to Chemistry*, Theoretical Chemistry and Computational Modelling, DOI 10.1007/978-94-007-6863-5_6,

6.1 Overlap Integrals

Operations and representations are merely theoretical constructs. What is actually observed are the *interactions*. In quantum mechanics, interactions are expressed as matrix elements of operators in a function space. When the operator is the unit operator, the matrix elements are just overlap integrals. These are the simplest form of interactions.

We start our analysis by examining symmetry selection rules for overlap integrals. Consider the overlap integral between the ith component of a function space which transforms according to the irrep Γ, and the kth component of another function space transforming as Γ'. The overlap integral, S_{ki}, is a scalar quantity and thus must be invariant under the action of linear symmetry operators acting on the functions.

$$S_{ki} = \langle \phi_k^{\Gamma'} | \psi_i^{\Gamma} \rangle = \hat{R} \langle \phi_k^{\Gamma'} | \psi_i^{\Gamma} \rangle \tag{6.1}$$

An integral being an infinite sum, the operator can be brought inside the bracket and then transform the bra and ket parts directly.

$$\hat{R} \langle \phi_k^{\Gamma'} | \psi_i^{\Gamma} \rangle = \langle \hat{R} \phi_k^{\Gamma'} | \hat{R} \psi_i^{\Gamma} \rangle = \sum_{jl} \bar{D}_{lk}^{\Gamma'}(R) D_{ji}^{\Gamma}(R) \langle \phi_l^{\Gamma'} | \psi_j^{\Gamma} \rangle \tag{6.2}$$

By summing over all $\hat{R} \in G$ and dividing by the group order one obtains a form to which the GOT can be applied.

$$\begin{aligned} \langle \phi_k^{\Gamma'} | \psi_i^{\Gamma} \rangle &= \frac{1}{|G|} \sum_{R \in G} \hat{R} \langle \phi_k^{\Gamma'} | \psi_i^{\Gamma} \rangle \\ &= \frac{1}{|G|} \sum_{jl} \left(\sum_R \bar{D}_{lk}^{\Gamma'}(R) D_{ji}^{\Gamma}(R) \right) \langle \phi_l^{\Gamma'} | \psi_j^{\Gamma} \rangle \\ &= \delta_{\Gamma' \Gamma} \delta_{ik} \frac{1}{\dim(\Gamma)} \sum_j \langle \phi_j^{\Gamma'} | \psi_j^{\Gamma} \rangle \end{aligned} \tag{6.3}$$

We now rewrite this result in terms of elements of the overlap matrix $\mathbb{S}$:

$$S_{ki} = \delta_{\Gamma' \Gamma} \delta_{ik} \frac{1}{\dim(\Gamma)} \sum_j S_{jj} = \delta_{\Gamma' \Gamma} \delta_{ik} \frac{1}{\dim(\Gamma)} \mathrm{Tr}(\mathbb{S}) \tag{6.4}$$

This simple derivation yields three important results:

1. Overlap integrals between functions which transform according to different irreps are zero.
2. Overlap integrals between functions which belong to different components of the same irrep are zero.
3. Overlap integrals between functions with the same symmetry properties, i.e. transforming as the *same component* of the *same irrep*, are independent of the component choice provided that both components are normalized.

These results clearly illustrate the importance of the GOT. It not only provides a selection rule at the level of the irreps, but also at the level of the components. Of course, the latter selection rule will work only if we ensured that the symmetry adaptation of the basis set has been carried out at the component level, as was explained in Sect. 5.3.

A further consequence is that SALCs on peripheral atom sites can quite often easily be derived from central symmetry-adapted orbitals. One simply has to make sure that the SALCs have the same nodal characteristics as the central functions, so as to guarantee maximal overlap. This is well illustrated in Fig. 4.4.

6.2 The Coupling of Representations

Overlap integrals are scalar products of a bra and a ket function. A general matrix element is an integral of the outer product of a bra, an operator, and a ket, giving rise to a triad of irreps. The evaluation of such elements is based on the *coupling* of irreps. This concept refers to the formation of a product space. The simplest example is the formation of a two-electron wavefunction, obtained by multiplying two one-electron functions. This section will be devoted entirely to the formation of such product spaces.

Consider two sets of orbitals, transforming as the irreps Γ_a and Γ_b respectively, each occupied by one electron. A two-electron wavefunction with electron 1 in the γ_a component of the first set, and electron 2 in the γ_b component of the second set is written as a simple product function: $|\Gamma_a\gamma_a(1)\rangle|\Gamma_b\gamma_b(2)\rangle$. Clearly, since the one-electron function spaces are invariants of the group, their product space is invariant, too. Now the question is to determine the symmetry of this new space. The recipe to find this symmetry can safely be based on the character theorem: first determine the character string for the product basis, and then carry out the reduction according to the character theorem. Symmetry operators are all-electron operators affecting all particles together; hence, the effect of a symmetry operation on a ket product is to transform both kets simultaneously.

$$\hat{R}\big(\big|\Gamma_a\gamma_a(1)\big\rangle\big|\Gamma_b\gamma_b(2)\big\rangle\big) = \sum_{\gamma_a'}\sum_{\gamma_b'} D^{\Gamma_a}_{\gamma_a'\gamma_a}(R)D^{\Gamma_b}_{\gamma_b'\gamma_b}(R)\big|\Gamma_a\gamma_a'(1)\big\rangle\big|\Gamma_b\gamma_b'(2)\big\rangle \quad (6.5)$$

The transformation of the product functions is thus expressed by a super matrix, each element of which is a product of two matrix elements for the individual orbital transformations. The trace of this super matrix is given by:

$$\begin{aligned}\chi^{\Gamma_a\times\Gamma_b}(R) &= \sum_{\gamma_a\gamma_b} D^{\Gamma_a}_{\gamma_a\gamma_a}(R)D^{\Gamma_b}_{\gamma_b\gamma_b}(R)\\ &= \chi^{\Gamma_a}(R)\chi^{\Gamma_b}(R) \end{aligned} \quad (6.6)$$

This is a gratifying result. The character of a product space is simply the product of the characters of the factor spaces. Accordingly, the symmetry of the product space

Table 6.1 Direct product of $E_g \times T_{2g}$ in O_h symmetry

O_h	$\hat{E}$	$8\hat{C}_3$	$6\hat{C}_2$	$6\hat{C}_4$	$3\hat{C}_2$	$\hat{i}$	$6\hat{S}_4$	$8\hat{S}_6$	$3\hat{\sigma}_h$	$6\hat{\sigma}_d$
E_g	2	−1	0	0	2	2	0	−1	2	0
T_{2g}	3	0	1	−1	−1	3	−1	0	−1	1
$E_g \times T_{2g}$	6	0	0	0	−2	6	0	0	−2	0
T_{1g}	3	0	−1	1	−1	3	1	0	−1	−1
T_{2g}	3	0	1	−1	−1	3	−1	0	−1	1

is identified as the *direct product* of the orbital irreps, and is denoted as $\Gamma_a \times \Gamma_b$. If both irreps are degenerate, the direct product will be reducible. Let c_Γ be the number of times that the irrep Γ occurs in the direct product:

$$\Gamma_a \times \Gamma_b = \sum_\Gamma c_\Gamma \Gamma \tag{6.7}$$

By straightforward application of the character theorem one obtains:

$$\begin{aligned} c_\Gamma &= \frac{1}{|G|} \sum_R \bar{\chi}^\Gamma(R) \chi^{\Gamma_a \times \Gamma_b}(R) \\ &= \frac{1}{|G|} \sum_R \bar{\chi}^\Gamma(R) \chi^{\Gamma_a}(R) \chi^{\Gamma_b}(R) \end{aligned} \tag{6.8}$$

Here we have, for the first time, a formula with a triad of irreps. This will form the basis for the symmetry evaluation of general matrix elements. The c_Γ coefficients are obtained by performing product manipulations on the character tables. As an example, Table 6.1 illustrates the reduction of the $E_g \times T_{2g}$ product in O_h, as given in Eq. (6.9). Product tables are given in Appendix E.

$$E_g \times T_{2g} = T_{1g} + T_{2g} \tag{6.9}$$

Let us now proceed with the two-electron problem and address the next question, which is that, after having determined which symmetry species are present, we should like to know what the corresponding two-electron wavefunctions look like, i.e. we should like to construct the SALCs. This construction does not pose any new problems; the projection operators that were introduced in Sect. 4.5 will do the job perfectly well. Some notation is important here. The product function will be written as:

$$\left|\Gamma\gamma(1,2)\right\rangle = \sum_{\gamma_a} \sum_{\gamma_b} c^{\Gamma\gamma}_{\gamma_a\gamma_b} \left|\Gamma_a\gamma_a(1)\right\rangle \left|\Gamma_b\gamma_b(2)\right\rangle \tag{6.10}$$

The combination coefficient is itself identified as a matrix element, by multiplying left and right with the one-electron bra functions and using orthonormality of the

basis orbitals.

$$c^{\Gamma}_{\gamma_a\gamma_b} = \left\langle \Gamma_a\gamma_a(1)\Gamma_b\gamma_b(2)|\Gamma\gamma(1,2)\right\rangle \equiv \langle \Gamma_a\gamma_a\Gamma_b\gamma_b|\Gamma\gamma\rangle \tag{6.11}$$

This coefficient is known as a Clebsch–Gordan (CG) coupling coefficient and denoted by the 3Γ bracket $\langle \Gamma_a\gamma_a\Gamma_b\gamma_b|\Gamma\gamma\rangle$. It indicates how the orbital irreps Γ_a and Γ_b have to be combined to yield a product ket that transforms as $|\Gamma\gamma\rangle$. The CG-coefficients can be determined by using projection operators. The results are listed in Appendix F. It is often possible to obtain these results by a simpler procedure. We illustrate this for the components of the T_{1g} two-electron state, obtained in Eq. (6.9). The z-component of this state is the only component that is totally symmetric under the $\hat{C}_4$ splitting field. It is clear that this symmetry can be obtained only by multiplying the $|e_g\epsilon\rangle$ and $|t_{2g}\zeta\rangle$ components, since these are both antisymmetric and thus will form a symmetric product. From here on we will adopt for the product functions the usual notation of small letters for the orbitals and capital letters for the coupled states. Hence:

$$|T_{1g}z\rangle = |e_g\epsilon\rangle|t_{2g}\zeta\rangle \tag{6.12}$$

The coupling coefficient $\langle E_g\epsilon T_{2g}\zeta|T_{1g}z\rangle$ is thus equal to 1. The x and y components may then immediately be obtained by applying the cyclic $\hat{C}_3$ generator. As an example for the x-component:

$$\begin{aligned} |T_{1g}x\rangle &= \hat{C}_3|T_{1g}z\rangle \\ &= \left(\hat{C}_3|e_g\epsilon\rangle\right)\left(\hat{C}_3|t_{2g}\zeta\rangle\right) \\ &= \left(-\frac{\sqrt{3}}{2}|e_g\theta\rangle - \frac{1}{2}|e_g\epsilon\rangle\right)|t_{2g}\xi\rangle \\ &= -\frac{\sqrt{3}}{2}|e_g\theta\rangle|t_{2g}\xi\rangle - \frac{1}{2}|e_g\epsilon\rangle|t_{2g}\xi\rangle \end{aligned} \tag{6.13}$$

Thus: $\langle\theta\xi|x\rangle = -\sqrt{3}/2$; $\langle\epsilon\xi|x\rangle = -1/2$. The resulting coupling coefficients are shown in Table 6.2.

6.3 Symmetry Properties of the Coupling Coefficients

The CG-coefficients in the finite point groups stem from Wigner's celebrated coupling coefficients for the spherical symmetry group [1]. Wigner proposed reformulating these coefficients in terms of more primitive $3j$ symbols, which contain, in a uniform way, the permutational properties of the spherical coupling coefficients. Several attempts have been made to define similar 3Γ symbols for the point group, but this requires the introduction of quite detailed phase conventions, which limits the efficiency of this formalism [2, 3]. We shall therefore not engage in a further

Table 6.2 The coupling coefficients for the direct product $E_g \times T_{2g}$ in O_h symmetry

$E_g \times T_{2g}$	T_{1g}			T_{2g}		
	x	y	z	ξ	η	ζ
$\|\theta\rangle\|\xi\rangle$	$-\frac{\sqrt{3}}{2}$	0	0	$-\frac{1}{2}$	0	0
$\|\theta\rangle\|\eta\rangle$	0	$\frac{\sqrt{3}}{2}$	0	0	$-\frac{1}{2}$	0
$\|\theta\rangle\|\zeta\rangle$	0	0	0	0	0	1
$\|\epsilon\rangle\|\xi\rangle$	$-\frac{1}{2}$	0	0	$\frac{\sqrt{3}}{2}$	0	0
$\|\epsilon\rangle\|\eta\rangle$	0	$-\frac{1}{2}$	0	0	$-\frac{\sqrt{3}}{2}$	0
$\|\epsilon\rangle\|\zeta\rangle$	0	0	1	0	0	0

factorization of the coupling coefficients, but, express the important symmetry properties of the couplings at the level of the brackets. Two guidelines will thereby be used: when dealing with coupling coefficients it is important to bear in mind that the coupling is based on the formation of a product, as we have illustrated in the preceding section, and, secondly, that we should treat the coupling coefficients as far as possible as ordinary brackets.

A direct consequence of the latter viewpoint is that the rules for complex conjugation of brackets apply:

$$\overline{\langle \Gamma_a \gamma_a \Gamma_b \gamma_b | \Gamma \gamma \rangle} = \langle \Gamma \gamma | \Gamma_a \gamma_a \Gamma_b \gamma_b \rangle \tag{6.14}$$

Being expansion coefficients of SALCs, the coupling coefficients also obey two orthogonality rules. Column-wise orthonormality results from the orthonormal properties of the coupled states.

$$\sum_{\gamma_a \gamma_b} \big\langle \Gamma' \gamma' | \Gamma_a \gamma_a \Gamma_b \gamma_b \big\rangle \langle \Gamma_a \gamma_a \Gamma_b \gamma_b | \Gamma \gamma \rangle = \delta_{\Gamma \Gamma'} \delta_{\gamma \gamma'} \tag{6.15}$$

In addition, the scalar products along rows are orthonormal, because of the orthonormal properties of the basic kets. Note that the summation runs over the irreps of the entire product space: $\Gamma \in \Gamma_a \times \Gamma_b$.

$$\sum_{\Gamma \gamma} \big\langle \Gamma_a \gamma_a' \Gamma_b \gamma_b' | \Gamma \gamma \big\rangle \langle \Gamma \gamma | \Gamma_a \gamma_a \Gamma_b \gamma_b \rangle = \delta_{\gamma_a' \gamma_a} \delta_{\gamma_b' \gamma_b} \tag{6.16}$$

The permutational properties of the CG-coefficients refer to interchange of the bra and ket irreps. If Γ_a and Γ_b are not equivalent, their ordering will not affect the symmetry of the coupled state, since the factors in the direct product commute:

$$\Gamma_a \times \Gamma_b = \Gamma_b \times \Gamma_a \tag{6.17}$$

We can therefore define the coupling coefficients in such a way that interchange of the coupled irreps leaves the coefficient invariant:

$$\Gamma_a \neq \Gamma_b : \langle \Gamma_a \gamma_a \Gamma_b \gamma_b | \Gamma \gamma \rangle \equiv \langle \Gamma_b \gamma_b \Gamma_a \gamma_a | \Gamma \gamma \rangle \tag{6.18}$$

If the coupled electrons are equivalent, i.e. belong *to the same shell*, the situation is different. In this case, $\Gamma_a = \Gamma_b$, and the direct product becomes a *direct square*. For non-equivalent irreps, exchange of the components γ_a and γ_b was not possible, because they refer to different irreps. However, when they are components of the same irrep, this exchange is an important symmetry of the product space. Indeed, the squared space can be split into two separate blocks, one block which contains product functions that are symmetric under exchange of the component labels and one block which is antisymmetric. This implies that we can define two separate sets of direct square coupling coefficients, which are either symmetric or antisymmetric under exchange of the labels, i.e.: $\langle \Gamma_a\gamma_a\Gamma_a\gamma_b|\Gamma\gamma\rangle = \pm\langle\Gamma_a\gamma_b\Gamma_a\gamma_a|\Gamma\gamma\rangle$. The symmetrized part of the direct square is denoted as $[\Gamma_a]^2$. For $n = \dim(\Gamma_a)$, the dimension of this subspace is equal to the number of symmetric combinations:

$$\dim\big([\Gamma_a]^2\big) = \sum_{\gamma_a} 1 + \sum_{\gamma_a<\gamma_b} 1 = n + n(n-1)/2 = n(n+1)/2 \tag{6.19}$$

On the other hand, if the coupling coefficients are antisymmetric under exchange of the labels, the coupled state belongs to the antisymmetrized direct square, denoted as $\{\Gamma_a\}^2$. This product space is restricted to combinations with $\gamma_a \neq \gamma_b$; its dimension is equal to $n(n-1)/2$. The characters for either part of the square can be determined separately. For the character of the $\{\Gamma_a\}^2$ part the derivation runs as follows: one first applies a symmetry operator to an arbitrary antisymmetric function. The ket product $|\Gamma_a\gamma_a(1)\rangle|\Gamma_a\gamma_b(2)\rangle$ will be abbreviated here as: $\gamma_a(1)\gamma_b(2)$.

$$\begin{aligned}
&\hat{R}\big(\gamma_a(1)\gamma_b(2) - \gamma_b(1)\gamma_a(2)\big) \\
&\quad= \sum_{\gamma'_a\gamma'_b} \big(\gamma'_a(1)\gamma'_b(2) - \gamma'_b(1)\gamma'_a(2)\big) D^{\Gamma_a}_{\gamma'_a\gamma_a}(R) D^{\Gamma_a}_{\gamma'_b\gamma_b}(R) \\
&\quad= \sum_{\gamma'_a\gamma'_b} \gamma'_a(1)\gamma'_b(2)\big(D^{\Gamma_a}_{\gamma'_a\gamma_a}(R) D^{\Gamma_a}_{\gamma'_b\gamma_b}(R) - D^{\Gamma_a}_{\gamma'_a\gamma_b}(R) D^{\Gamma_a}_{\gamma'_b\gamma_a}(R)\big) \\
&\quad= \frac{1}{2}\sum_{\gamma'_a\gamma'_b} \big(\gamma'_a(1)\gamma'_b(2) - \gamma'_b(1)\gamma'_a(2)\big)\big(D^{\Gamma_a}_{\gamma'_a\gamma_a}(R) D^{\Gamma_a}_{\gamma'_b\gamma_b}(R) - D^{\Gamma_a}_{\gamma'_a\gamma_b}(R) D^{\Gamma_a}_{\gamma'_b\gamma_a}(R)\big)
\end{aligned} \tag{6.20}$$

Taking the trace then yields:

$$\begin{aligned}
\chi^{\{\Gamma_a\}^2}(R) &= \frac{1}{2}\sum_{\gamma_a\gamma_b} \big(D^{\Gamma_a}_{\gamma_a\gamma_a}(R) D^{\Gamma_a}_{\gamma_b\gamma_b}(R) - D^{\Gamma_a}_{\gamma_a\gamma_b}(R) D^{\Gamma_a}_{\gamma_b\gamma_a}(R)\big) \\
&= \frac{1}{2}\left(\big(\chi^{\Gamma_a}(R)\big)^2 - \sum_{\gamma_a} D^{\Gamma_a}_{\gamma_a\gamma_a}\big(R^2\big)\right) \\
&= \frac{1}{2}\big(\big(\chi^{\Gamma_a}(R)\big)^2 - \chi^{\Gamma_a}\big(R^2\big)\big)
\end{aligned} \tag{6.21}$$

Table 6.3 Direct square $H_g \times H_g$ in I_h symmetry

I_h	$\hat{E}$	$12\hat{C}_5$	$12\hat{C}_5^2$	$20\hat{C}_3$	$15\hat{C}_2$	$\hat{i}$	$12\hat{S}_{10}$	$12\hat{S}_{10}^3$	$20\hat{S}_6$	$15\hat{\sigma}$
χ^{H_g}	5	0	0	−1	1	5	0	0	−1	1
$\chi^{H_g{}^2}$	25	0	0	1	1	25	0	0	1	1
$\chi^{H_g}(R^2)$	5	0	0	−1	5	5	0	0	−1	5
$\chi^{[H_g]^2}$	15	0	0	0	3	15	0	0	0	3
$\chi^{\{H_g\}^2}$	10	0	0	1	−2	10	0	0	1	−2

The trace for the symmetrized product is then found by subtracting the trace in Eq. (6.21) from the total trace for the direct product.

$$\begin{aligned}\chi^{[\Gamma_a]^2}(R) &= \chi^{\Gamma_a{}^2}(R) - \chi^{\{\Gamma_a\}^2}(R) \\ &= \frac{1}{2}\left(\left(\chi^{\Gamma_a}(R)\right)^2 + \chi^{\Gamma_a}\left(R^2\right)\right)\end{aligned} \tag{6.22}$$

In Table 6.3 these quantities are given for the direct product $H_g \times H_g$ in icosahedral symmetry. The product resolution is as follows:

$$H_g \times H_g = [A_g + G_g + 2H_g] + \{T_{1g} + T_{2g} + G_g\} \tag{6.23}$$

Note that this product contains one totally-symmetric irrep, notably in the symmetrized part. In general, for irreps with real characters the totally-symmetric irrep, Γ_0, appears in a direct square only once. This can easily be derived from Eq. (6.8). When Γ_a is an irrep with *real characters*, one has:

$$\begin{aligned}\left\langle \chi^{\Gamma_0} | \chi^{\Gamma_a \times \Gamma_b} \right\rangle &= \sum_R \bar{\chi}^{\Gamma_0}(R)\chi^{\Gamma_a}(R)\chi^{\Gamma_b}(R) \\ &= \sum_R \chi^{\Gamma_a}(R)\chi^{\Gamma_b}(R) \\ &= |G|\delta_{\Gamma_a\Gamma_b}\end{aligned} \tag{6.24}$$

In the case of irreps that can be represented by *real transformation matrices*, it is possible to show that this totally-symmetric irrep will belong to the symmetrized part. In order to apply the character theorem to Eq. (6.22), the following intermediate result is needed:

$$\begin{aligned}\sum_R \chi^{\Gamma_a}\left(R^2\right) &= \sum_R \sum_i \left[\mathbb{D}^{\Gamma_a}(R) \times \mathbb{D}^{\Gamma_a}(R)\right]_{ii} \\ &= \sum_R \sum_i \sum_j D_{ij}^{\Gamma_a}(R) D_{ji}^{\Gamma_a}(R) \\ &= \frac{|G|}{\dim(\Gamma_a)} \sum_i \sum_j \delta_{ij} = |G|\end{aligned} \tag{6.25}$$

In order to arrive at this result we have made use of the GOT, on the assumption that the $\mathbb{D}$ matrices are real. Combining the results of Eqs. (6.24) and (6.25) with

Eq. (6.22) then leads to the conclusion that the unique totally-symmetric irrep belongs to the symmetrized part of the direct square:

$$\frac{1}{|G|}\langle \chi^{\Gamma_0} | \chi^{[\Gamma_a]^2} \rangle = \frac{1}{2|G|} \sum_R \chi^{\Gamma_0}(R) \left[\chi^{\Gamma_a{}^2}(R) + \chi^{\Gamma_a}(R^2) \right] = 1 \tag{6.26}$$

For irreps with real characters, but transformation matrices that cannot be all real, the unique totally-symmetric product appears in the antisymmetrized part. This is the case for spin representations, which will be dealt with in Chap. 7. In summary, as far as complex-conjugation properties are concerned, we have three kinds of irreps:

1. Irreps with real characters, and for which all $\mathbb{D}(R)$ transformation matrices can be put in real form. In this case: $\Gamma_0 \in [\Gamma_a]^2$.
2. Irreps with real characters, but which cannot be represented by transformation matrices that are all real. In this case $\Gamma_0 \in \{\Gamma_a\}^2$.
3. Irreps with complex characters. In this case there is always a complex-conjugate irrep, and $\Gamma_0 \in \Gamma \times \bar{\Gamma}$.

Equation (6.23) further exemplifies a case of *product multiplicity*. This is when an irrep occurs more than once in the decomposition of a direct product. Both the H_g and G_g irreps appear twice in the direct product $H_g \times H_g$. In the point groups product multiplicity is quite rare. It occurs only in the icosahedral group for the products $G \times H$ and $H \times H$, as well for spin representations in cubic and icosahedral symmetries. Product multiplicity means that there are different coupling schemes for arriving at the product states. Each of these "channels" corresponds to a separate set of CG coupling coefficients. There are several ways of obtaining linearly-independent sets of coupling coefficients. For the separation of the two G_g irreps in Eq. (6.23) symmetrization of the product space is sufficient, since the symmetrized and antisymmetrized parts each contain one G_g. This strategy does not work for the two H_g irreps, which are both the result of symmetrized coupling. In this case, more elaborate splitting schemes have been constructed, based *inter alia* on higher symmetries [4, 5].

Last but not least, we should consider the relationship between coupling coefficients where irreps from bra and ket parts are interchanged. We shall limit the discussion here to the simplified case in which all ingredients of the coupling are taken to be real. A case with complex irreps will be treated in Chap. 7. Consider two related couplings: $\Gamma_a \times \Gamma_b = \Gamma$ and $\Gamma \times \Gamma_b = \Gamma_a$. The corresponding expansion coefficients are scalar matrix elements and are thus invariant under the group action. By importing the group action inside the brackets, as we have frequently done before, we obtain a set of equations in the CG-coefficients:

$$\langle \Gamma_a \gamma_a \Gamma_b \gamma_b | \Gamma \gamma \rangle = \sum_{\gamma_a' \gamma_b' \gamma} \left[\frac{1}{|G|} \sum_R \bar{D}^{\Gamma_a}_{\gamma_a' \gamma_a}(R) \bar{D}^{\Gamma_b}_{\gamma_b' \gamma_b}(R) D^{\Gamma}_{\gamma' \gamma}(R) \right] \langle \Gamma_a \gamma_a' \Gamma_b \gamma_b' | \Gamma \gamma' \rangle \tag{6.27}$$

$$\langle \Gamma\gamma\,\Gamma_b\gamma_b|\Gamma_a\gamma_a\rangle = \sum_{\gamma_a'\gamma_b'\gamma}\left[\frac{1}{|G|}\sum_R D^{\Gamma_a}_{\gamma_a'\gamma_a}(R)\bar{D}^{\Gamma_b}_{\gamma_b'\gamma_b}(R)\bar{D}^{\Gamma}_{\gamma'\gamma}(R)\right]\langle \Gamma\gamma'\,\Gamma_b\gamma_b'|\Gamma_a\gamma_a'\rangle \tag{6.28}$$

These equations form a system of homogeneous linear equations from which the coupling coefficients can be obtained. At present, we shall use this result only in the simplified case where all components have been chosen to be real, so that Eqs. (6.27) and (6.28) form the same system of equations.[1] From this it follows that the corresponding coupling coefficients will be proportional to each other, independent of the components; hence:

$$\langle \Gamma_a\gamma_a\,\Gamma_b\gamma_b|\Gamma\gamma\rangle = x\langle \Gamma\gamma\,\Gamma_b\gamma_b|\Gamma_a\gamma_a\rangle \tag{6.29}$$

The proportionality constant can be determined by summing the square of the coefficients over all components and using the normalization result from Eq. (6.15).

$$\sum_{\gamma_a\gamma_b\gamma}\left|\langle \Gamma_a\gamma_a\,\Gamma_b\gamma_b|\Gamma\gamma\rangle\right|^2 = x^2\sum_{\gamma_a\gamma_b\gamma}\left|\langle \Gamma\gamma\,\Gamma_b\gamma_b|\Gamma_a\gamma_a\rangle\right|^2$$

$$\dim(\Gamma) = x^2\dim(\Gamma_a) \tag{6.30}$$

The permutation of irreps between bra and ket in the CG-coefficients thus requires a uniform dimensional renormalization:

$$\big[\dim(\Gamma)\big]^{-1/2}\langle \Gamma_a\gamma_a\,\Gamma_b\gamma_b|\Gamma\gamma\rangle = \pm\big[\dim(\Gamma_a)\big]^{-1/2}\langle \Gamma\gamma\,\Gamma_b\gamma_b|\Gamma_a\gamma_a\rangle \tag{6.31}$$

The renormalization leaves a phase factor undetermined. This phase factor is the same for the entire coupling table, and thus can be chosen in arbitrarity. As an example, in the group O (see Appendix F), the coefficients $\langle T_2\xi\,T_1x|E\theta\rangle$ and $\langle E\theta\,T_1x|T_2\xi\rangle$ are related as follows:

$$\frac{1}{\sqrt{2}}\langle T_2\xi\,T_1x|E\theta\rangle = \frac{1}{\sqrt{3}}\langle E\theta\,T_1x|T_2\xi\rangle = -\frac{1}{2} \tag{6.32}$$

Here the phase was chosen to be $+1$.

6.4 Product Symmetrization and the Pauli Exchange-Symmetry

In principle, the T_{1g} and T_{2g} coupled two-electron states, which we obtained in Table 6.2 of the previous section, could apply to the case of the $(t_{2g})^1(e_g)^1$ excited states of a d^2 transition-metal ion in an octahedral ligand field, which splits the d

[1] The general case with complex irreps is exemplified for the coupling of spin representations in Sect. 7.4.

orbitals into a t_{2g} and an e_g shell. However, these coupled descriptions are not yet sufficient, since they make a distinction between electron 1, which resides in the t_{2g} orbital, and electron 2, which was promoted to the e_g level. The fundamental symmetry requirement that electrons must be indistinguishable is thus not fulfilled. The operator that permutes the two electrons is represented as $\hat{P}_{12}$:

$$\hat{P}_{12}\big|\Gamma\gamma(1,2)\big\rangle = \big|\Gamma\gamma(2,1)\big\rangle = \sum_{\gamma_a}\sum_{\gamma_b}\langle\Gamma_a\gamma_a\Gamma_b\gamma_b|\Gamma\gamma\rangle\big|\Gamma_a\gamma_a(2)\big\rangle\big|\Gamma_b\gamma_b(1)\big\rangle \quad (6.33)$$

The $|\Gamma\gamma(1,2)\rangle$ and $|\Gamma\gamma(2,1)\rangle$ states will have exactly the same symmetries, since the factors in the direct product commute:

$$\Gamma_a \times \Gamma_b = \Gamma_b \times \Gamma_a \quad (6.34)$$

As a result, $\hat{P}_{12}$ commutes with the spatial symmetry operators, and we can symmetrize the coupled states with respect to the electron permutation. The permutation operator is the generator of the symmetric group, S_2, which has only two irreps, one symmetric and one antisymmetric, corresponding, respectively, to the plus and minus combination in Eq. (6.35).

$$\begin{aligned}|\Gamma\gamma;\pm\rangle &= \frac{1}{\sqrt{2}}\big[\big|\Gamma\gamma(1,2)\big\rangle \pm \big|\Gamma\gamma(2,1)\big\rangle\big] \\ &= \frac{1}{\sqrt{2}}\sum_{\gamma_a}\sum_{\gamma_b}\langle\Gamma_a\gamma_a\Gamma_b\gamma_b|\Gamma\gamma\rangle \\ &\quad\times\big[\big|\Gamma_a\gamma_a(1)\big\rangle\big|\Gamma_b\gamma_b(2)\big\rangle \pm \big|\Gamma_b\gamma_b(1)\big\rangle\big|\Gamma_a\gamma_a(2)\big\rangle\big]\end{aligned} \quad (6.35)$$

These states have distinct permutation symmetries, and spatial symmetry operators cannot mix $+$ and $-$ states. This is a very general property of multi-particle states, to which no exceptions are known.

On the other hand the permutation symmetry of multi-electron wavefunctions is restricted by the Pauli principle.

Theorem 11 *The total wavefunction should be antisymmetric with respect to exchange of any pair of electrons. Hence, in the symmetric group S_2, or, for an n-electron system, the symmetric group, S_n, the total wavefunction should change sign under odd permutations, i.e. under permutations that consist of an odd number of transpositions of two elements, and should remain invariant under even permutations.*

Until now we have limited ourselves to the spatial part of the wavefunction. So far, only the antisymmetrized part obeys the Pauli principle. However, the principle places a requirement only on the *total* wavefunction. This also involves a spin part, which should be multiplied by the orbital part. Anticipating the results of Chap. 7, we here provide the spin functions for a two-electron system. Spin functions are characterized by a spin quantum number, S, and a component, M_S, in the range

$\{-S, -S+1, -S+2, \ldots, S-1, S\}$. The total number of components, hence the dimension of the spin-space for a given S, is equal to $2S+1$. This number is called the spin multiplicity. For a two-electron system, S can be 0 or 1; hence, there is one singlet state, and there are three components belonging to a triplet state. In a $|SM_S\rangle$ notation they are given by:

$$\begin{aligned} |0,0\rangle &= \frac{1}{\sqrt{2}}\big[\alpha(1)\beta(2) - \beta(1)\alpha(2)\big] \\ |1,1\rangle &= \alpha(1)\alpha(2) \\ |1,0\rangle &= \frac{1}{\sqrt{2}}\big[\alpha(1)\beta(2) + \beta(1)\alpha(2)\big] \\ |1,-1\rangle &= \beta(1)\beta(2) \end{aligned} \tag{6.36}$$

These functions also exhibit permutation symmetry: the triplet functions are symmetric under exchange of the two particles, while the singlet function is antisymmetric under such an exchange. The total wavefunction can thus always be put in line with the Pauli principle by combining the coupled orbital states with spin states of opposite permutation symmetry. Altogether we can thus construct four states: ${}^1T_{1g}$, ${}^1T_{2g}$, ${}^3T_{1g}$, ${}^3T_{2g}$. This set of four states, totalling 24 wavefunctions, forms a *manifold*, representing all the coupled states resulting from the $(t_{2g})^1(e_g)^1$ configuration. The dimension of the manifold is equal to the product of the six possible t_{2g} substates (including spin), and the four possible e_g substates. In this case, where the coupling involves electrons belonging to different shells, the Pauli principle does not restrict the total dimension of the manifold, since all combinations remain possible. All states can be written as linear combinations of Slater determinants. As an example, for the $|{}^1T_{1g}z\rangle$ state, one writes:

$$\begin{aligned} \big|{}^1T_{1g}z\big\rangle &= \frac{1}{\sqrt{2}}\big(\big|\epsilon(1)\big\rangle\big|\zeta(2)\big\rangle + \big|\epsilon(2)\big\rangle\big|\zeta(1)\big\rangle\big)\frac{1}{\sqrt{2}}\big[\alpha(1)\beta(2) - \beta(1)\alpha(2)\big] \\ &= \frac{1}{\sqrt{2}}\big|(\epsilon\alpha)(\zeta\beta)\big| - \frac{1}{\sqrt{2}}\big|(\epsilon\beta)(\zeta\alpha)\big| \end{aligned} \tag{6.37}$$

The situation is different when coupling two equivalent electrons; these are electrons that belong to *the same shell*. In this case, the coupled states are already eigenfunctions of the exchange operator as a result of the special symmetrization properties of the coupling coefficients for direct squares. Equation (6.10) will take the following form:

$$\begin{aligned} |\Gamma\gamma(1,2)\rangle = \sum_{\gamma_a\gamma_b}\langle\gamma_a\gamma_b|\Gamma\gamma\rangle\big|\gamma_a(1)\big\rangle\big|\gamma_b(2)\big\rangle = \sum_{\gamma_a}\langle\gamma_a\gamma_a|\Gamma\gamma\rangle\big|\gamma_a(1)\big\rangle\big|\gamma_a(2)\big\rangle \\ + \sum_{\gamma_a<\gamma_b}\big[\langle\gamma_a\gamma_b|\Gamma\gamma\rangle\big|\gamma_a(1)\big\rangle\big|\gamma_b(2)\big\rangle + \langle\gamma_b\gamma_a|\Gamma\gamma\rangle\big|\gamma_b(1)\big\rangle\big|\gamma_a(2)\big\rangle\big] \end{aligned} \tag{6.38}$$

Now, if the product representation belongs to the symmetrized square, $\Gamma \in [\Gamma_a]^2$, this result simplifies to:

$$|\Gamma\gamma\rangle = \sum_{\gamma_a} \langle \gamma_a \gamma_a | \Gamma\gamma \rangle \big|\gamma_a(1)\big\rangle \big|\gamma_a(2)\big\rangle + \sum_{\gamma_a < \gamma_b} \langle \gamma_a \gamma_b | \Gamma\gamma \rangle \Big(\big|\gamma_a(1)\big\rangle \big|\gamma_b(2)\big\rangle + \big|\gamma_b(1)\big\rangle \big|\gamma_a(2)\big\rangle \Big) \tag{6.39}$$

Hence, this function is symmetric under the $\hat{P}_{12}$ operator. It also obeys the normalization condition of Eq. (6.15). It should always be multiplied by an antisymmetric singlet spin-function in order to obey the Pauli exclusion principle. On the other hand, if the product representation belongs to the antisymmetrized square, $\Gamma \in \{\Gamma_a\}^2$, the coupled state is given by:

$$|\Gamma\gamma\rangle = \sum_{\gamma_a < \gamma_b} \langle \gamma_a \gamma_b | \Gamma\gamma \rangle \Big(\big|\gamma_a(1)\big\rangle \big|\gamma_b(2)\big\rangle - \big|\gamma_b(1)\big\rangle \big|\gamma_a(2)\big\rangle \Big) \tag{6.40}$$

This function is antisymmetric under the $\hat{P}_{12}$ operator, and should be multiplied by a symmetric triplet spin-function in order to obey the Pauli principle. As an example, for the $(e_g)^2$ configuration the allowed states are:

$$e_g \times e_g = [A_{1g} + E_g] + \{A_{2g}\} \Rightarrow {}^1A_{1g} + {}^1E_g + {}^3A_{2g} \tag{6.41}$$

For equivalent electrons the Pauli principle thus really does function as an exclusion principle, since the coupled states are either triplets or singlets, depending on their symmetrization. The dimension of the manifold is given by the binomial coefficient, where q is the number of equivalent substates (including spin), and n is the number of electrons:

$$\binom{q}{n} = \frac{q!}{n!(q-n)!} \tag{6.42}$$

For the $(e_g)^2$ problem, one has $n = 2$ and $q = 4$; there are thus six two-electron states in this configuration (see Eq. (6.41)).

As a special result, we examine the symmetry of the maximal spin-multiplicity ground state of a system with a half-filled shell. The shell consists of the components $|f_1\rangle \cdots |f_n\rangle$, transforming according to the irrep Γ_a, and each will be occupied by one electron with α spin. The ground state corresponds to a single determinant:

$$|\Psi\rangle = |f_1\alpha \cdots f_2\alpha| = \frac{1}{\sqrt{n!}} \sum_{\sigma \in S_n} \mathrm{sgn}(\sigma) \big[f_1\alpha(\sigma_1) \cdots f_n\alpha(\sigma_n) \big] = \frac{1}{\sqrt{n!}} \sum_{\sigma \in S_n} \mathrm{sgn}(\sigma) \big[f_{\sigma_1}\alpha(1) \cdots f_{\sigma_n}\alpha(n) \big] \tag{6.43}$$

Here, $\sigma \in S_n$ is an element of the permutation group of the n electron labels, and $\mathrm{sgn}(\sigma)$ is its parity.[2] Equation (6.43) indicates that this permutation can equally well be applied to the component labels, since the determinant is invariant under matrix transposition. We can now calculate the matrix element in the symmetry operator:

$$\begin{aligned}\langle\Psi|\hat{R}|\Psi\rangle &= \frac{1}{n!}\sum_{\sigma,\pi\in S_n}\mathrm{sgn}(\sigma)\mathrm{sgn}(\pi)\big[\langle f_{\sigma_1}\alpha(1)|\hat{R}|f_{\pi_1}\alpha(1)\rangle\cdots\langle f_{\sigma_n}\alpha(n)|\hat{R}|f_{\pi_n}\alpha(n)\rangle\big]\\ &= \frac{1}{n!}\sum_{\sigma,\pi\in S_n}\mathrm{sgn}(\sigma)\mathrm{sgn}(\pi)\big[D^{\Gamma_a}_{\sigma_1\pi_1}(R)\cdots D^{\Gamma_a}_{\sigma_n\pi_n}(R)\big]\\ &= \sum_{\lambda\in S_n}\mathrm{sgn}(\lambda)\big[D^{\Gamma_a}_{1\lambda_1}(R)\cdots D^{\Gamma_a}_{n\lambda_n}(R)\big]\\ &= \det\big(\mathbb{D}^{\Gamma_a}\big)\end{aligned} \tag{6.44}$$

In this equation we have used the result from Eq. (2.8), which identified matrix elements over symmetry operators as elements of the representation matrix. The double summation over permutations covers the permutation group twice and could be reduced to a single sum. The result indicates that the spatial symmetry of the half-filled shell ground state transforms as the determinant of the irrep of the shell. This is also called the *determinantal* representation. For the e_g shell the determinantal irrep is A_{2g}. The shell ground state is thus a ${}^3A_{2g}$.

6.5 Matrix Elements and the Wigner–Eckart Theorem

A general interaction element is a bracket around an operator. Each of the three ingredients, bra, ket, and operator, can be put in symmetry-adapted form, so that it transforms according to a given irrep. Moreover, provided that the symmetry adaptation is done properly, not only the irrep itself but also the subrepresentation is well defined. Altogether, the matrix element will thus be characterized by six symmetry labels, as: $\langle\psi^{\Omega}_{\omega}|O^{\Lambda}_{\lambda}|\phi^{\Gamma}_{\gamma}\rangle$. The labels imply that the symmetry behaviour of each of these ingredients is fully known:

$$\begin{aligned}\hat{R}\big|\psi^{\Omega}_{\omega}\big| &= \sum_{\omega'}\bar{D}^{\Omega}_{\omega'\omega}(R)\big|\psi^{\Omega}_{\omega'}\big|\\ \hat{R}\big|\phi^{\Gamma}_{\gamma}\big\rangle &= \sum_{\gamma'}D^{\Gamma}_{\gamma'\gamma}(R)\big|\phi^{\Gamma}_{\gamma'}\big\rangle\\ \hat{R}\big|O^{\Lambda}_{\lambda}\big|R^{-1} &= \sum_{\lambda'}D^{\Lambda}_{\lambda'\lambda}(R)\big|O^{\Lambda}_{\lambda'}\big|\end{aligned} \tag{6.45}$$

[2] Any permutation can be expressed as a sequence of transpositions of two elements. If the total number of transpositions is even, $\mathrm{sgn}(\sigma) = +1$; if it is odd, $\mathrm{sgn}(\sigma) = -1$. See also Sect. 3.3.

Note that the general form of the operator $|O_\lambda^\Lambda|$ refers to a component of an irreducible set. Such a set of operators is usually referred to as a *tensor operator*. Obvious examples are the components of the electric or magnetic dipole-moment operators. The Wigner–Eckart theorem introduces a symmetry factorization, which simplifies the evaluation of matrix elements.

Theorem 12 *A matrix element, involving a tensor operator, may be factorized into a product of an intrinsic scalar part and an appropriate* 3Γ *coupling coefficient.*

The scalar constant is denoted by $\langle \psi^\Omega \parallel O^\Lambda \parallel \phi^\Gamma \rangle$, and is called the *reduced matrix element*.

$$\left\langle \psi_\omega^\Omega \middle| O_\lambda^\Lambda | \phi_\gamma^\Gamma \right\rangle = \left\langle \psi^\Omega \parallel O^\Lambda \parallel \phi^\Gamma \right\rangle \langle \Omega\omega | \Lambda\lambda\Gamma\gamma \rangle \tag{6.46}$$

To prove this theorem, one first considers the coupling of two ingredients of the matrix element, and then compares the result with the third one. We thus first consider the coupling of the operator and the ket. The transformation of their product does indeed correspond to the super matrix which is due to the direct product $\Lambda \times \Gamma$.

$$\hat{R}\left| O_\lambda^\Lambda | \phi_\gamma^\Gamma \right\rangle = \hat{R}\left| O_\lambda^\Lambda | \hat{R}^{-1}\hat{R} | \phi_\gamma^\Gamma \right\rangle = \sum_{\lambda'} \sum_{\gamma'} D_{\lambda'\lambda}^\Lambda(R) D_{\gamma'\gamma}^\Gamma(R) | O_{\lambda'}^\Lambda \left| \phi_{\gamma'}^\Gamma \right\rangle \tag{6.47}$$

This means that we couple the tensor operator and the ket to form product entities:

$$\left| (O\phi)_\pi^\Pi \right\rangle = \sum_{\lambda'} \sum_{\gamma'} \left| O_{\lambda'}^\Lambda | \phi_{\gamma'}^\Gamma \right\rangle \left\langle \Lambda\lambda'\Gamma\gamma' | \Pi\pi \right\rangle \tag{6.48}$$

We now invert this equation, using the unitary properties of the coupling coefficients, to yield:

$$\left| O_\lambda^\Lambda | \phi_\gamma^\Gamma \right\rangle = \sum_{\Pi'} \sum_{\pi'} \left| (O\phi)_{\pi'}^{\Pi'} \right\rangle \left\langle \Pi'\pi' | \Lambda\lambda\Gamma\gamma \right\rangle \tag{6.49}$$

Then we combine this expression with the bra.

$$\left\langle \psi_\omega^\Omega | O_\lambda^\Lambda | \phi_\gamma^\Gamma \right\rangle = \sum_{\Pi'} \sum_{\pi'} \left\langle \psi_\omega^\Omega | (O\phi)_{\pi'}^{\Pi'} \right\rangle \left\langle \Pi'\pi' | \Lambda\lambda\Gamma\gamma \right\rangle \tag{6.50}$$

The matrix elements on the right-hand side are now in fact reduced to an overlap integral where the direct product irreps are compared with the irrep of the bra. Hence, the selection rules for the overlap integrals apply:

$$\left\langle \Omega\omega | (O\phi)_{\pi'}^{\Pi'} \right\rangle = \delta_{\Omega,\Pi'}\delta_{\omega\pi'} \frac{1}{\dim(\Omega)} \sum_{\omega'} \left\langle \Omega\omega' \middle| (O\phi)_{\omega'}^{\Omega'} \right\rangle \equiv \left\langle \psi^\Omega \parallel O^\Lambda \parallel \phi^\Gamma \right\rangle \tag{6.51}$$

The trace summation in this equation is identified as a scalar interaction constant, which is represented by the reduced matrix element.

Combination of Eqs. (6.50) and (6.51) then yields the Wigner–Eckart theorem of Eq. (6.46), where the total interaction is the product of a scalar interaction constant and a CG coupling coefficient. The former refers to the interaction itself, the latter extracts the transformation properties. In case of product multiplicity, there will be one reduced matrix element for every coupling channel, and the matrix element is decomposed into a sum over the channels. The Wigner–Eckart theorem or matrix-element theorem is at the heart of most chemical applications of group theory. It provides an elegant method for separating interactions into an intrinsic part and a part that depends only on the symmetry of the problem under consideration.

An important consequence of the matrix element theorem concerns the definition of selection rules. An interaction will be forbidden if the corresponding coupling coefficient in the Wigner–Eckart theorem is zero. The conditions that control the zero values of the coupling coefficients are called *triangular conditions*, since they involve the combination of three irreps. Two kinds of triangular conditions must be taken into account:

1. Selectivity on the representations: an interaction element is forbidden if the coupling of the three irreps involved is zero, i.e. if the direct product of the operator and ket parts does not include the irrep of the bra.

$$\Omega \notin \Lambda \times \Gamma \tag{6.52}$$

   The triad of the three irreps may also be seen as a triple direct product, $\bar{\Omega} \times \Lambda \times \Gamma$, where the bra irrep appears in its complex-conjugate form. Equation (6.8) can now also be read as the character overlap between the totally-symmetric irrep and the triple product. Accordingly, the selection rule of Eq. (6.52) can also be reformulated as: an interaction will be forbidden if the triple product of the irreps does not contain the totally-symmetric irrep.

$$\Gamma_0 \notin \bar{\Omega} \times \Lambda \times \Gamma \tag{6.53}$$

2. Selectivity on the subrepresentations: subrepresentations that are defined in a splitting field must obey the triangular conditions for the subduced irreps in the corresponding subgroup.

6.6 Application: The Jahn–Teller Effect

In 1937 Jahn and Teller made the claim that degenerate states of molecules are intrinsically unstable [6, 7].

Theorem 13 *Non-linear molecules in a spatially-degenerate electronic state are subject to spontaneous symmetry-breaking forces that distort the molecule to a geometry of lower symmetry, where the degeneracy is removed.*

The theorem is based on a perturbation of the Hamiltonian by small displacements of the nuclei. A high-symmetry geometry is chosen as the origin, and the nuclear displacements are described by normal modes which transform as irreps of the point group. The nuclear positions are parameters in the electronic Hamiltonian. One has, to second-order:

$$\begin{aligned}\mathcal{H} &= \mathcal{H}_0 + \mathcal{H}' \\ \mathcal{H}' &= \sum_{Q_{\Gamma\gamma}} \left(\frac{\partial \mathcal{H}}{\partial Q_{\Gamma\gamma}}\right)_0 Q_{\Gamma\gamma} + \frac{1}{2} \sum_{Q_{\Gamma\gamma}} \sum_{Q_{\Gamma'\gamma'}} \left(\frac{\partial^2 \mathcal{H}}{\partial Q_{\Gamma\gamma} \partial Q_{\Gamma'\gamma'}}\right)_0 Q_{\Gamma\gamma} Q_{\Gamma'\gamma'}\end{aligned} \tag{6.54}$$

The partial derivatives with respect to the normal modes will affect only the electrostatic V_{Ne} term in the Hamiltonian. These operators are thus electrostatic one-electron operators. At the coordinate origin, the electronic state is degenerate, and is described by a set of wavefunctions, $|\Gamma_a \gamma_a\rangle$, where Γ_a is a degenerate irrep. The energies as functions of the coordinates are obtained by diagonalizing the Hamiltonian matrix, $\mathbb{H}$, with elements:

$$H_{\gamma_a \gamma_b} = \langle \Gamma_a \gamma_a | \mathcal{H} | \Gamma_a \gamma_b \rangle = E_0 \delta_{\gamma_a \gamma_b} + \left\langle \Gamma_a \gamma_a \middle| \mathcal{H}' \middle| \Gamma_a \gamma_b \right\rangle \tag{6.55}$$

The matrix in $\mathcal{H}'$ is also called the Jahn–Teller (JT) matrix. The linear terms in this matrix are of type:

$$\left\langle \Gamma_a \gamma_a \middle| \left(\frac{\partial \mathcal{H}}{\partial Q_{\Gamma\gamma}}\right)_0 Q_{\Gamma\gamma} \middle| \Gamma_a \gamma_b \right\rangle = \left\langle \Gamma_a \gamma_a \middle| \frac{\partial \mathcal{H}}{\partial Q_{\Gamma\gamma}} \middle| \Gamma_a \gamma_b \right\rangle_0 Q_{\Gamma\gamma} \tag{6.56}$$

We have used the fact that the integration in this matrix element runs over electronic coordinates, and does not affect the nuclear coordinates. The Wigner–Eckart theorem can be applied to derive the selection rules. Since the Hamiltonian is invariant under the elements of the symmetry group, the transformation properties of the operator part in this matrix element will be determined by the partial derivatives, $\partial / \partial Q_{\Gamma\gamma}$. As we have seen in Sect. 1.3, a partial derivative in a variable has the same transformation properties as the variable itself.[3] The operator part is thus given by:

$$\left\langle \Gamma_a \gamma_a \middle| \frac{\partial \mathcal{H}}{\partial Q_{\Gamma\gamma}} \middle| \Gamma_a \gamma_b \right\rangle_0 = \langle \Gamma_a \parallel \Gamma \parallel \Gamma_a \rangle \langle \Gamma_a \gamma_a | \Gamma \gamma \Gamma_a \gamma_b \rangle \tag{6.57}$$

The coupling coefficient on the right-hand side of Eq. (6.57) restricts the symmetry of the nuclear displacements to the direct square of the irrep of the electronic wavefunction. This selection rule is made even more stringent by time-reversal symmetry. The Hamiltonian is based on displacement of nuclear charges, and not on momenta, so as an operator it is time-even or real.[4] For spatially-degenerate irreps, which are

[3] For complex variables, variable and derivative have complex-conjugate transformation properties.

[4] The general time-reversal selection rules are discussed in Sect. 7.6.

of the first kind, i.e. can be represented by real functions, JT matrix elements can thus be chosen to be entirely real, which implies:

$$\left\langle \Gamma_a \gamma_a | \mathcal{H}' | \Gamma_a \gamma_b \right\rangle = \left\langle \Gamma_a \gamma_b | \mathcal{H}' | \Gamma_a \gamma_a \right\rangle \tag{6.58}$$

Combining this result with Eq. (6.57) implies that the coupling coefficients, to first-order, should obey:

$$\langle \Gamma_a \gamma_a | \Gamma \gamma \, \Gamma_a \gamma_b \rangle = \langle \Gamma_a \gamma_b | \Gamma \gamma \, \Gamma_a \gamma_a \rangle \tag{6.59}$$

In view of Eq. (6.31) this condition can be rewritten as:

$$\langle \Gamma_a \gamma_a \Gamma_a \gamma_b | \Gamma \gamma \rangle = \langle \Gamma_a \gamma_b \Gamma_a \gamma_a | \Gamma \gamma \rangle \tag{6.60}$$

The JT distortion modes are thus restricted to the symmetrized square of the degenerate irrep of the electronic state, minus the totally-symmetric modes, since these cannot lower the symmetry:

$$\Gamma \in \left([\Gamma_a \times \Gamma_a] - \Gamma_0 \right) \tag{6.61}$$

Modes that obey this selection rule, are said to be *JT active*. The evaluation of the second-order matrix elements requires two steps. One first couples the two distortion modes to a composite tensor operator: $|\Omega\omega|$.

$$\left| \frac{\partial^2 \mathcal{H}}{\partial Q_{\Gamma\gamma} \partial Q_{\Gamma'\gamma'}} \right| = \sum_{\Omega\omega} |\Omega\omega| \left\langle \Omega\omega | \Gamma\gamma \, \Gamma'\gamma' \right\rangle \tag{6.62}$$

The second-order matrix element then becomes:

$$\begin{aligned} &\left\langle \Gamma_a \gamma_a \left| \frac{\partial^2 \mathcal{H}}{\partial Q_{\Gamma\gamma} \partial Q_{\Gamma'\gamma'}} \right| \Gamma_a \gamma_b \right\rangle_0 \\ &\quad = \sum_{\Omega\omega} \langle \Gamma_a \parallel \Omega \parallel \Gamma_a \rangle \left\langle \Omega\omega | \Gamma\gamma \, \Gamma'\gamma' \right\rangle \langle \Gamma_a \gamma_a | \Omega\omega \Gamma_a \gamma_b \rangle \end{aligned} \tag{6.63}$$

The second-order elements thus are related to a product of two 3Γ symbols.[5] A special element arises when Ω is totally symmetric. In this case, the coupling coefficients are given by:

$$\begin{aligned} \left\langle \Gamma_0 | \Gamma\gamma \, \Gamma'\gamma' \right\rangle &= \frac{1}{\sqrt{\dim(\Gamma)}} \delta_{\Gamma\Gamma'} \delta_{\gamma\gamma'} \\ \langle \Gamma_a \gamma_a | \Gamma_0 \Gamma_a \gamma_b \rangle &= \delta_{\gamma_a \gamma_b} \end{aligned} \tag{6.64}$$

[5] Such combinations can be cast in a higher-order symbol, known as 6Γ symbol, by analogy with the $6j$ coupling coefficients in atomic spectroscopy.

The second-order expressions then are reduced to a diagonal matrix element:

$$\begin{aligned}&\langle \Gamma_a \parallel \Gamma_0 \parallel \Gamma_a\rangle\langle \Gamma_0|\Gamma\gamma\Gamma'\gamma'\rangle\langle \Gamma_a\gamma_b|\Gamma_0\Gamma_a\gamma_b\rangle \\ &\quad = \frac{1}{\sqrt{\dim(\Gamma)}}\langle \Gamma_a \parallel \Gamma_0 \parallel \Gamma_a\rangle\delta_{\Gamma\Gamma'}\delta_{\gamma\gamma'}\delta_{\gamma_a\gamma_b} = K_\Gamma\delta_{\Gamma\Gamma'}\delta_{\gamma\gamma'}\delta_{\gamma_a\gamma_b} \qquad (6.65)\end{aligned}$$

K_Γ in this equation is the harmonic force-constant. It gives rise to a constant diagonal term which provides an attractive potential around the minimum and keeps the surface bound at larger distances from the origin. The general expression for the potential-energy surface then becomes:

$$E_k(Q) = E_0 + \sum_\Gamma \frac{1}{2}K_\Gamma\left(\sum_\gamma Q^2_{\Gamma\gamma}\right) + \varepsilon_k(Q) \qquad (6.66)$$

Here, $\varepsilon_k(Q)$ represents the kth root of the Hamiltonian matrix. This equation describes a surface with multiple sheets, one for each root, which cross in the high-symmetry origin. In its simplest form the Hamiltonian can be restricted to the linear terms only. In the second-order approximation non-totally-symmetric second-order terms will also be included.

The prototype of the JT surface is the celebrated *Mexican hat* potential, which describes the effect of the twofold-degenerate cubic or trigonal E state. A typical example is the ${}^2E_g$ ground state of octahedral Cu^{2+} complexes, with $(t_{2g})^6(e_g)^3$ configuration. The JT-active mode in this case is restricted to an e_g mode, corresponding to the symmetrized square.

$$[E_g \times E_g] - A_{1g} = E_g \qquad (6.67)$$

This distortion mode consists of the tetragonal and orthorhombic stretchings, which we already encountered as vibrational modes of UF_6, and are depicted in Fig. 6.1. By use of the appropriate $\langle Ei|Ejk\rangle$ coupling coefficients the JT matrix can easily be derived. The force element is defined as:

$$F_E = \left\langle E\theta\left|\frac{\partial\mathcal{H}}{\partial Q_\theta}\right|E\theta\right\rangle \qquad (6.68)$$

The matrix then becomes:

$$\mathbb{H} = \left(E_0 + \frac{1}{2}K_E\left(Q_\theta^2 + Q_\epsilon^2\right)\right)\begin{bmatrix}1 & 0\\ 0 & 1\end{bmatrix} + F_E\begin{bmatrix}Q_\theta & Q_\epsilon\\ Q_\epsilon & -Q_\theta\end{bmatrix} \qquad (6.69)$$

To diagonalize this Hamiltonian, it is convenient to transform to cylindrical coordinates $\{\rho, \varphi\}$:

$$\begin{aligned}Q_\theta &= \rho\cos\varphi\\ Q_\epsilon &= \rho\sin\varphi\end{aligned} \qquad (6.70)$$

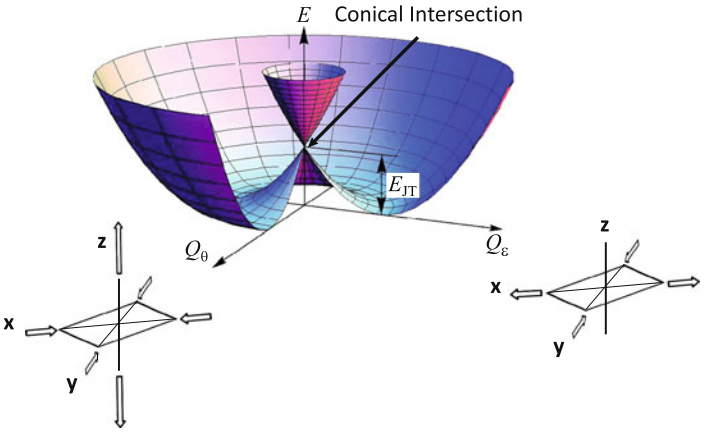

Fig. 6.1 The Mexican hat potential-energy surface of the $E \times e$ linear JT problem. The nuclear displacement coordinates are the tetragonal elongation, Q_θ, and the orthorhombic in-plane distortion, Q_ϵ

Then the secular equation of the force element matrix in Eq. (6.69) becomes:

$$\varepsilon_k^2 - F_E^2 \rho^2 \cos^2\varphi - F_E^2 \rho^2 \sin^2\varphi = 0 \tag{6.71}$$

Two roots are found, which are independent of the angular coordinate. The corresponding eigenfunctions are:

$$\begin{aligned} \epsilon_1 = F_E \rho \longrightarrow |\psi_1\rangle &= \cos\frac{\varphi}{2}|E\theta\rangle + \sin\frac{\varphi}{2}|E\epsilon\rangle \\ \epsilon_2 = -F_E \rho \longrightarrow |\psi_2\rangle &= -\sin\frac{\varphi}{2}|E\theta\rangle + \cos\frac{\varphi}{2}|E\epsilon\rangle \end{aligned} \tag{6.72}$$

The surface consists of two sheets and exhibits rotational symmetry.

$$\begin{aligned} E_\pm &= E_0 + \frac{1}{2}K_E\rho^2 \pm F_E\rho \\ &= E_0 + \frac{1}{2}K_E\left(Q_\theta^2 + Q_\epsilon^2\right) \pm F_E\sqrt{Q_\theta^2 + Q_\epsilon^2} \end{aligned} \tag{6.73}$$

A cross section of this surface looks like a two-well potential, with two displaced parabolæ. The depth of the well is called the JT stabilization energy:

$$E_{JT} = -\frac{F_E^2}{2K_E} \tag{6.74}$$

In the 2D space of the active modes these parabolæ revolve around the centre, giving rise to the Mexican hat appearance. At the origin this surface has the shape of a conical intersection, indicating that the high-symmetry point is unstable, and will spontaneously relax to the circular trough surrounding the degeneracy [8]. The

distorted system in the trough orbits around the origin. This motion is a *pseudo*-rotation, i.e. it is not a rotation of the molecular frame, but a gradual redistribution of the distortions between the Cartesian directions. We illustrate this in Fig. 6.2. The starting point is at $\varphi = 0$, in the direction of the Q_θ mode. In this mode the z-axis is elongated, and the xy-plane is contracted. A counterclockwise rotation activates the orthorhombic Q_ϵ mode, while the tetragonal Q_θ mode is receding. This introduces a difference between the x- and y-axes: the distortion in the x-direction becomes more pronounced, while the y-axis contracts further. At the same time the elongation of the z-axis diminishes. At an angle of 60° the x- and z-axes are both elongated to an equal extent, giving rise to a weak xz-plane and a strong y-axis. At the 90° point the Q_θ contribution vanishes, and the distortion is orthorhombic, with a short y-axis, an elongated x-axis, and an undistorted z-axis. At an angle of 120° we reach the point where the x-axis is weak, and the perpendicular yz-plane is strong. We thus have regained an elongated tetragonal configuration, but the elongation has been rotated from the z-axis to the x-axis. Continuing now at 240° we shall have travelled another third of the trough and reoriented the tetragonal axis along the y-direction. We can also follow the wavevector along the trough. If it is assumed that $F_E < 0$, the lower eigenfunction will be the $|\psi_1\rangle$ eigenfunction of Eq. (6.72). In the starting elongated tetragonal configuration the ground state coincides with the $|E\theta\rangle$ basis function. By the time we have reached the orthorhombic configuration at $\varphi = 90°$, the ground state has rotated by only half that angle and equals $1/\sqrt{2}(|E\theta\rangle + |E\epsilon\rangle)$. At 180°, we reach a structure which is tetragonally compressed along the z-direction. Accordingly, the Q_θ mode has changed sign, in contrast to the eigenfunction, where $|E\theta\rangle$ is replaced by $|E\epsilon\rangle$. The observation of rotational symmetry is an unexpected feature, which is not related to the point group, but which stems from the limitation of the JT Hamiltonian to linear terms. To describe this symmetry we first reformulate the force element Hamiltonian in Eq. (6.69) in Dirac notation:

$$\mathcal{H}' = F_E\big(Q_\theta\big[|E\theta\rangle\langle E\theta| - |E\epsilon\rangle\langle E\epsilon|\big] + Q_\epsilon\big[|E\theta\rangle\langle E\epsilon| + |E\epsilon\rangle\langle E\theta|\big]\big) \tag{6.75}$$

The angular momentum operator, corresponding to a rotation in coordinate space, is given by:

$$\mathcal{L} = \frac{\partial}{\partial\varphi} = \frac{\partial Q_\epsilon}{\partial\varphi}\frac{\partial}{\partial Q_\epsilon} + \frac{\partial Q_\theta}{\partial\varphi}\frac{\partial}{\partial Q_\theta} = Q_\theta\frac{\partial}{\partial Q_\epsilon} - Q_\epsilon\frac{\partial}{\partial Q_\theta} \tag{6.76}$$

The partial derivatives were obtained from Eq. (6.70). The commutator of this operator with the Hamiltonian is:

$$\big[\mathcal{L}, \mathcal{H}'\big] = F_E\big(-Q_\epsilon\big[|E\theta\rangle\langle E\theta| - |E\epsilon\rangle\langle E\epsilon|\big] + Q_\theta\big[|E\theta\rangle\langle E\epsilon| + |E\epsilon\rangle\langle E\theta|\big]\big) \tag{6.77}$$

Surprisingly, this commutator does not vanish. This is an important observation, which directly points to the vibrational-electronic or *vibronic* coupling between the distortion modes and the electronic wavevector. When the system rotates around the origin in coordinate space, not only are the coordinates changing, but the wavevector is also rotating simultaneously, so we must also provide an angular momentum

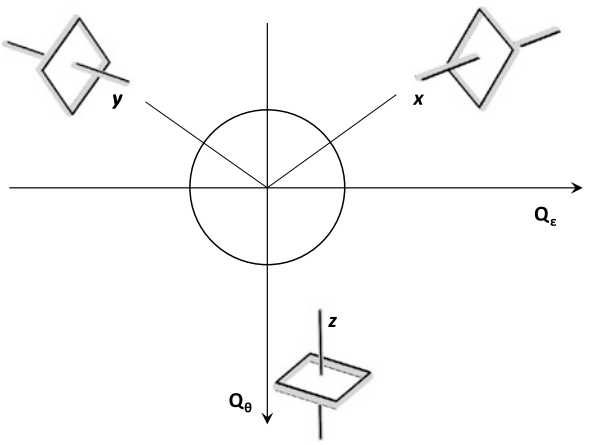

Fig. 6.2 Rotation of the distortion in the trough of the Mexican hat. Along the Q_θ coordinate the complex is elongated along its z-axis. Rotation around the centre in the direction of Q_ϵ will shorten the z-axis and increase the x-axis. At an angle of revolution of 120° a tetragonally elongated structure is again found, but this time with the elongation along the x-direction, and similarly at 240°, with the elongation along the y-axis

operator for a rotation in the function space (see [9]). We can construct this by analogy with Eq. (6.76), but with an important amendment: as we have argued while discussing Fig. 6.2, the coordinates rotate twice as quickly as the wavevector, and hence a prefactor of $1/2$ is required!

$$\mathcal{S} = \frac{1}{2}\big(|E\theta\rangle\langle E\epsilon| - |E\epsilon\rangle\langle E\theta|\big) \tag{6.78}$$

Only in this case does the total momentum operator $\mathcal{J} = \mathcal{L} + \mathcal{S}$ commute with the Hamiltonian:

$$\big[\mathcal{J}, \mathcal{H}'\big] = \big[\mathcal{L}, \mathcal{H}'\big] + \big[\mathcal{S}, \mathcal{H}'\big] = 0 \tag{6.79}$$

As the reader will have noticed, we have made use of the standard spectroscopic symbols for orbital angular momentum, spin momentum, and total momentum. Vibronic coupling is indeed analogous to coupling of spin and orbit momenta in cylindrical molecules. To form the vibronic wavefunction, describing the dynamics of the Mexican hat system, the electronic state has to be combined with nuclear wavefunctions. If the JT effect is pronounced, the vibronic levels take the form of a radial oscillator, describing transverse oscillations in the bottom of the through, and pseudo-rotational levels, describing the longitudinal motion along the bottom of the trough. The total vibronic wavefunction should of course be single-valued after a full turn around the trough, which takes the system back to the starting point. Hence, since the electronic part changes sign after a full turn, the vibrational part should also show a compensating sign change. This is indeed the case: the pseudo-rotational levels are characterized by half-integral angular momentum [10].

6.7 Application: Pseudo-Jahn–Teller interactions

Pseudo-JT interactions (PJT) refer to the second-order vibronic coupling between electronic states which are separated by a gap [11]. In this section we describe the

case of a non-degenerate ground state, $|\psi_{\Sigma\sigma}\rangle$, which is coupled to an excited manifold. The Hamiltonian is identical to the expression in Eq. (6.54). Application of the selection rules shows that the diagonal contribution, $\langle\psi_{\Sigma\sigma}|\mathcal{H}|\psi_{\Sigma\sigma}\rangle$, is limited to the totally-symmetric operator associated with the harmonic restoring-force, as in Eq. (6.66). Perturbation theory further provides interactions between the ground and excited states. These interactions are usually limited to first-order contributions, which give rise to a quadratic coordinate dependence. Hence one has, to second-order in the displacements:

$$\begin{aligned} E(Q) = E_0 + \sum_{\Gamma} \frac{1}{2} K_{\Gamma} \left(\sum_{\gamma} Q_{\Gamma\gamma}^2 \right) \\ + \sum_{\Lambda\lambda} \sum_{\Gamma\gamma} \frac{|\langle\psi_{\Lambda\lambda}|\frac{\partial\mathcal{H}}{\partial Q_{\Gamma\gamma}}|\psi_{\Sigma\sigma}\rangle_0|^2}{E_0 - E_{\Lambda}} Q_{\Gamma\gamma}^2 \end{aligned} \tag{6.80}$$

where we have used the property that the Hamiltonian matrix is hermitian. The selection rule in this process resides with the matrix elements in the enumerator of the bilinear term. The vibronic operator must couple ground and excited states; hence, it is required that their triple direct product contains the totally-symmetric irrep:

$$\Gamma_0 \in \bar{\Gamma}_{\Lambda} \times \Gamma \times \Sigma \tag{6.81}$$

Applying the Wigner–Eckart theorem to the matrix element yields:

$$\left\langle \psi_{\Lambda\lambda} \middle| \frac{\partial\mathcal{H}}{\partial Q_{\Gamma\gamma}} \middle| \psi_{\Sigma\sigma} \right\rangle_0 = \langle\Lambda\lambda|\Gamma\gamma\,\Sigma\sigma\rangle\langle\Lambda \parallel \Gamma \parallel \Sigma\rangle \tag{6.82}$$

The sum over the λ components of the excited state, transforming as the Λ irrep, can be simplified by using the orthonormality property of the coupling coefficients from Eq. (6.16).

$$\begin{aligned} \sum_{\lambda\in\Lambda} \frac{|\langle\psi_{\Lambda\lambda}|\frac{\partial\mathcal{H}}{\partial Q_{\Gamma\gamma}}|\psi_{\Sigma\sigma}\rangle_0|^2}{E_0 - E_{\Lambda}} &= \sum_{\lambda\in\Lambda} \frac{|\langle\Lambda\lambda|\Gamma\gamma\,\Sigma\sigma\rangle\langle\Lambda \parallel \Gamma \parallel \Sigma\rangle|^2}{E_0 - E_{\Lambda}} \\ &= \frac{|\langle\Lambda \parallel \Gamma \parallel \Sigma\rangle|^2}{E_0 - E_{\Lambda}} \end{aligned} \tag{6.83}$$

Note that in case of a non-degenerate ground state the product $\Gamma \times \Sigma$ yields only one irrep, since the norm of the product character string equals the order of the group.

$$\left\langle \chi^{\Gamma\times\Sigma} | \chi^{\Gamma\times\Sigma} \right\rangle = \left\langle \chi^{\Gamma}\chi^{\Sigma} | \chi^{\Gamma}\chi^{\Sigma} \right\rangle = \left\langle \chi^{\Gamma} | \chi^{\Gamma} \right\rangle = |G| \tag{6.84}$$

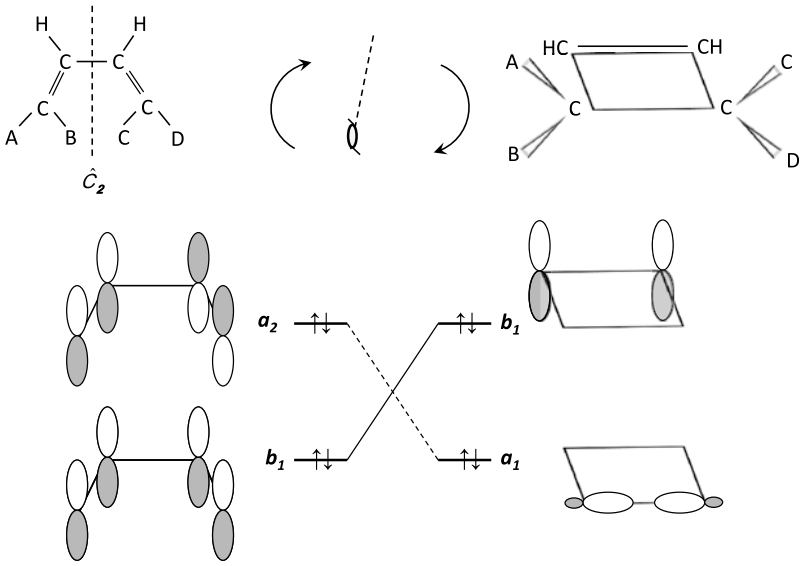

Fig. 6.3 Ring closure of *cis*-butadiene to *cyclo*-butene. In C_{2v} symmetry there is a symmetry mismatch between the a_2 and a_1 occupied orbitals. Vibronic orbital coupling requires a concerted mechanism, based on a conrotatory ring closure, which conserves only the $\hat{C}_2$ axis

The summation over $\lambda \in \Lambda$ thus covers the entire product space of $\Gamma \times \Sigma$. Combining the sum rule of Eq. (6.83) with the total expression for the PJT, one finds:

$$E(Q) = E_0 + \sum_{\Gamma} \left\{ \frac{1}{2} K_{\Gamma} + \sum_{\Lambda} \frac{|\langle \Lambda \parallel \Gamma \parallel \Sigma \rangle|^2}{E_0 - E_{\Lambda}} \right\} \left(\sum_{\gamma} Q_{\Gamma\gamma}^2 \right) \tag{6.85}$$

Hence, when the ground state is non-degenerate, the first-order dependence of the energy on symmetry-lowering displacement vanishes, and the second-order term contains two contributions: the diagonal harmonic force constant, which is always positive, and the bilinear relaxation term, which is always negative. If the excited states are close in energy to the ground state, and if the vibronic coupling is strong, the relaxation term may be dominant, and a second-order symmetry-breaking effect will result. This is known as the pseudo-JT effect. There are two main applications of this effect: in geometry optimization, and in reaction dynamics.

In reaction dynamics the PJT may be responsible for stereoselectivity, because of the selection rules for vibronic coupling matrix elements. Via these relaxation matrix elements the Wigner–Eckart theorem is at the basis of the Woodward–Hoffmann rules [12]. We shall not discuss these rules in general, but consider some simple illustrations, related to electrocyclic reactions.[6] Take as a simple example the ring closure of *cis*-butadiene, as illustrated in Fig. 6.3. The relevant occupied orbitals are

[6] Based on [13].

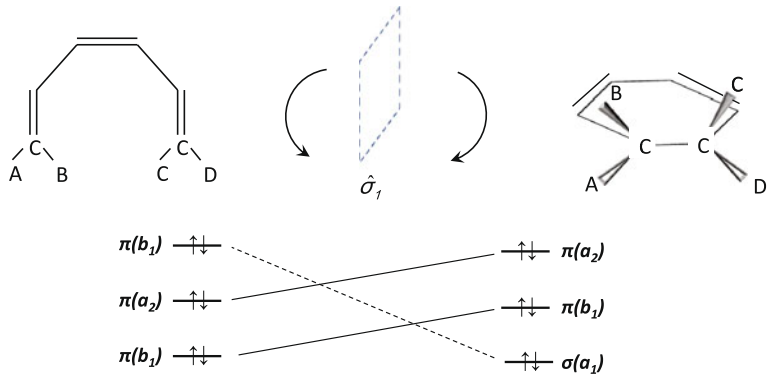

Fig. 6.4 Ring closure of *cis*-1, 3, 5-hexatriene to *cyclo*-hexadiene. In C_{2v} symmetry there is a symmetry mismatch between the b_1 and a_1 occupied orbitals. Vibronic orbital coupling requires a concerted mechanism, based on a disrotatory ring closure, which conserves only the $\hat{\sigma}_1$ plane

the π-bonds in the reagent, and the remaining π- and newly formed σ-bonds in the product. As the diagram shows, in the common C_{2v} point group there is a mismatch between the symmetries. In order for the reaction to occur, the reaction coordinate has to reduce the symmetry so that the a_2-orbital can interchange with an a_1-orbital. This interchange is taking place via a PJT mechanism which couples the a_2 occupied orbital to an a_1 virtual orbital in the reagent. As the reaction coordinate proceeds, this coupling is intensified and leads to an interchange of both. The relevant matrix element is thus an orbital vibronic coupling element:

$$\left\langle a_2 \left| \frac{\partial \mathcal{H}}{\partial Q_{\Gamma\gamma}} \right| a_1 \right\rangle \neq 0 \tag{6.86}$$

Hence, a distortion coordinate is required which transforms as $a_2 \times a_1 = a_2$. The coordinate with this symmetry is the one that destroys the symmetry planes but keeps the twofold axis. This is typically a *conrotatory* reaction, where the extremal carbon atoms rotate simultaneously in the same sense, to form the σ-bond. Ring closure of substituted butadienes thus follows a conrotatory reaction stereochemistry, at least if the reaction is concerted.

This ring-closure selection rule is further confirmed by the closure reaction for the cis-1, 3, 5 hexatriene to 1, 3-cyclohexadiene, as illustrated in Fig. 6.4. Here, a b_1-orbital has to interchange with a virtual orbital of a_1 symmetry. The selection takes thus place at the level of the orbital matrix element:

$$\left\langle b_1 \left| \frac{\partial \mathcal{H}}{\partial Q_{\Gamma\gamma}} \right| a_1 \right\rangle \neq 0 \tag{6.87}$$

Clearly, the distortion coordinate should now be of $b_1 \times a_1 = b_1$ symmetry, and this corresponds to the *disrotatory* mode, which destroys the $\hat{C}_2$ axis but keeps the vertical reflection plane.

6.8 Application: Linear and Circular Dichroism

Selection rules are of primary importance in spectroscopy, where they provide direct evidence concerning the nature of excited states. As an application, we study the linear and circular dichroism of tris-chelate transition-metal complexes [14]. The prototype is a divalent ruthenium complex with three $2,2'$-bipyridyl ligands, which is an important chromophore for energy conversion. In this section we shall describe the charge transfer and intra-ligand transitions of this type of complex. The linear dichroism (LD) spectrum measures the absorption of the chromophore under plane-polarized incident light for different orientations of the polarization with respect to the molecular frame. This requires that the molecules should be embedded in an oriented phase, such as a crystalline host. Circular dichroism (CD) measures the difference in absorption between left and right circularly polarized light. Since this is based on the intrinsic helicity of the molecule, it can be performed in non-oriented medium, such as a solution.

As always, we start the treatment by making a simple sketch of the structure. Two sets of Cartesian axes are relevant. In the usual octahedral coordinate system the x, y, z-axes coincide with the metal-ligand bond directions, assuming that the ligator atoms form a perfect octahedron. In addition, in Fig. 3.6 of Chap. 3 a primed x', y', z'-coordinate system was introduced, which is adapted to the tris-chelate geometry. The z'-axis is along the threefold direction, and the x' axis is oriented along a twofold axis, coinciding with the bisector of the positive x and the negative y axes. Next, we determine the point group, which in the present case is D_3. This is a rotational group, which implies that the molecule is chiral. The figure shows the Δ-enantiomer.[7] Thirdly, we define the functional basis. The relevant orbitals are the metal t_{2g} orbitals, which are fully occupied in the Ru^{2+} ground state, and the frontier orbitals on the ligand. For conjugated bidentate ligands, such as $2,2'$-bipyridyl (bipy) or 2, 4-pentanedionate (also named "acetylacetonate", $acac^-$), the frontier orbitals are of π-type. The essential parts of these orbitals are the contributions on the ligator atoms. These are either symmetric or antisymmetric with respect to the twofold axis through the bidentate ligand, as shown in Fig. 6.5. Following Orgel, we denote them as χ- or ψ-type, respectively [15]. The standard techniques of characters and projection operators yield SALCs for all these basis sets. The results are shown in Table 6.4. For the e-irrep the components are labelled as e_θ and e_ϵ, following the standard canonical format. As a splitting field we use the twofold axis along x'. Finally, we also include in the table the symmetries of the transition dipoles, which are the operators for the optical transitions. This completes the groundwork for the symmetry analysis.

[7] In tris-chelate complexes Δ refers to a right-handed (*dextro*) helix. A left-handed helix (*lævo*) is denoted as Λ.

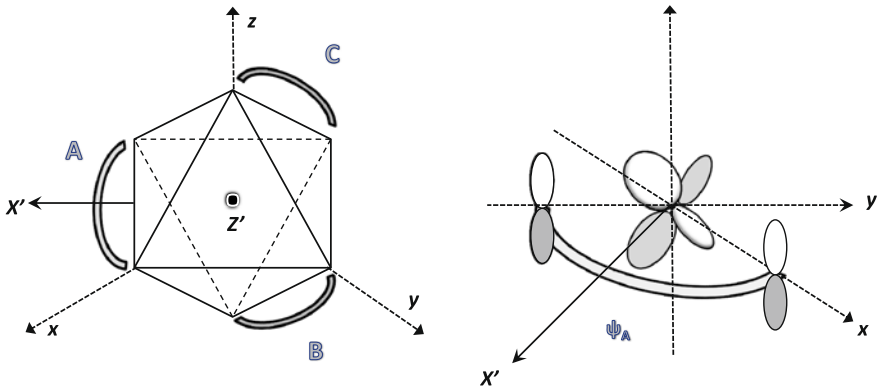

Fig. 6.5 Δ-enantiomer of tris-chelate octahedral complex of D_3 symmetry. The xyz-coordinate system passes through the ligator atoms; the primed coordinate system has the z'-direction along the threefold axis, and x' on a twofold axis through ligand A. The ligand orbital shown on the right is of ψ-type: it is antisymmetric under a rotation about the twofold axis through the ligator bridge. The ψ orbital on ligand A interacts with the $\frac{1}{\sqrt{2}}(d_{xz} - d_{yz})$-combination on the metal

Table 6.4 Symmetry-adapted zeroth-order metal and ligand orbital functions

t_{2g}-orbitals		dipole moments
$\|a_1\rangle = \frac{1}{\sqrt{3}}(d_{xy} + d_{xz} + d_{yz})$		$a_2 : \mu_{z'}$
$\|e_\theta\rangle = \frac{1}{\sqrt{6}}(-2d_{xy} + d_{xz} + d_{yz})$		$e_\theta : \mu_{x'}$
$\|e_\epsilon\rangle = \frac{1}{\sqrt{2}}(d_{xz} - d_{yz})$		$e_\epsilon : \mu_{y'}$
ψ-orbitals	χ-orbitals	
$\|a_2\rangle = \frac{1}{\sqrt{3}}(\|\psi_A\rangle + \|\psi_B\rangle + \|\psi_C\rangle)$	$\|a_1\rangle = \frac{1}{\sqrt{3}}(\|\chi_A\rangle + \|\chi_B\rangle + \|\chi_C\rangle)$	
$\|e_\theta\rangle = \frac{1}{\sqrt{2}}(\|\psi_C\rangle - \|\psi_B\rangle)$	$\|e_\theta\rangle = \frac{1}{\sqrt{6}}(2\|\chi_A\rangle - \|\chi_B\rangle - \|\chi_C\rangle)$	
$\|e_\epsilon\rangle = \frac{1}{\sqrt{6}}(2\|\psi_A\rangle - \|\psi_B\rangle - \|\psi_C\rangle)$	$\|e_\epsilon\rangle = \frac{1}{\sqrt{2}}(\|\chi_B\rangle - \|\chi_C\rangle)$	

Linear Dichroism

The linear dichroism is associated with the metal-to-ligand charge-transfer (CT) transitions [16]. Dipole-allowed transitions between the orbitals are governed by the appropriate D_3 coupling coefficients. However, since both donor and acceptor orbitals, as well as the transition operators, each involve two irreps, several symmetry-independent coupling channels are possible. As is often the case in transition-metal spectroscopy, it is not sufficient to identify the reduced matrix elements; for a deeper understanding a further development of the model is often required to compare the reduced matrix elements. In the case of the CT bands the model of Day and Sanders offers just that little extra [17]. According to this simple model, a charge-transfer

(CT) transition between metal and ligand gains intensity when the relevant metal and ligand orbitals interact.

We first calculate the interaction terms between the metal and isolated ligand orbitals. The bipy ligand has low-lying unoccupied levels of ψ-character, which form π-acceptor interactions with the metal t_{2g} orbitals. Let H_π represent the elementary interaction between a ligand ψ orbital and a metal t_{2g} orbital, directed towards one ligator. The allowed interactions are then obtained by cyclic permutation:

$$\begin{aligned} H_\pi &= \langle d_{xz}|\mathcal{H}|\psi^A\rangle = -\langle d_{yz}|\mathcal{H}|\psi^A\rangle \\ &= \langle d_{xy}|\mathcal{H}|\psi^B\rangle = -\langle d_{xz}|\mathcal{H}|\psi^B\rangle \\ &= \langle d_{yz}|\mathcal{H}|\psi^C\rangle = -\langle d_{xy}|\mathcal{H}|\psi^C\rangle \end{aligned} \tag{6.88}$$

In order to apply the model of Day and Sanders, we now consider the CT transition between the ligand orbital on A and the t_{2g} combination that interacts with it. As shown in Fig. 6.5, the ψ^A-acceptor orbital is antisymmetric with respect to the $\hat{C}_2^{x'}$ axis and antisymmetric in the xy-plane. The only matching t_{2g} combination on the metal is the $|e_\epsilon(t_{2g})\rangle$ component (see Table 6.4). In the local C_{2v} symmetry, $|\psi_A\rangle$ and $|e_\epsilon(t_{2g})\rangle$ both transform as b_2 (taking the horizontal plane as the local $\hat{\sigma}_1$). Their interaction element is expressed as:

$$\langle e_\epsilon(t_{2g})|\mathcal{H}|\psi^A\rangle = \frac{1}{\sqrt{2}}\langle d_{xz} - d_{yz}|\mathcal{H}|\psi^A\rangle = \sqrt{2}H_\pi \tag{6.89}$$

We now consider the transition dipole moment between these orbitals along the x' direction, with $\mu_{x'} = -\mathrm{e}x'$. In C_{2v} symmetry this component transforms as a_1, while $\mu_{y'}$ and $\mu_{z'}$ are antisymmetric with respect to the $\hat{C}_2^{x'}$ axis. According to the Wigner–Eckart theorem, a transition dipole between two b_2 orbitals must transform as the direct product $b_2 \times b_2 = a_1$; hence, only the x'- component will be dipole-allowed. In a perturbative approach, which takes into account the symmetry-allowed interaction between the metal and ligand orbitals, one has:

$$\mu\left(e_\epsilon(t_{2g}) \to \psi^A\right) = \langle e_\epsilon(t_{2g})|\mu_{x'}|\psi^A\rangle - \frac{\langle e_\epsilon(t_{2g})|\mathcal{H}|\psi^A\rangle}{E_\psi - E_{t_{2g}}}\langle\psi^A|\mu_{x'}|\psi^A\rangle \tag{6.90}$$

In this expression the first term is the *contact* term between the zeroth-order orbitals. The second term is the *transfer* term, arising from the interaction between the donor and acceptor orbitals. In the simplified model of Day and Sanders this term is the dominant contribution. The transfer-dipole matrix element in Eq. (6.90) is approximated as the dipole length of the transferred charge, which we will represent as μ_A.

$$\langle\psi^A|\mu_{x'}|\psi^A\rangle = -\mathrm{e}\langle\psi^A|x'|\psi^A\rangle \approx -\mathrm{e}|\mathbf{R}_A| = -\mathrm{e}\rho \equiv \mu_A \tag{6.91}$$

where $\mathbf{R}_A$ is the radius vector from the origin to the centre of ligand A, with length ρ. Since the three ligands are equivalent, we further write:

$$\mu_A = \mu_B = \mu_C \equiv \mu^\perp \tag{6.92}$$

The three vectors of the ligand positions can be expressed in a row notation for the primed x', y', z' coordinate system as:

$$\begin{aligned} \boldsymbol{R}_A &= \rho(1,0,0) \\ \boldsymbol{R}_B &= \rho\left(-\frac{1}{2}, \frac{\sqrt{3}}{2}, 0\right) \\ \boldsymbol{R}_C &= \rho\left(-\frac{1}{2}, -\frac{\sqrt{3}}{2}, 0\right) \end{aligned} \tag{6.93}$$

The transfer term then becomes:

$$\boldsymbol{\mu}\left(e_\epsilon(t_{2g}) \rightarrow \psi^A\right) = -\mathrm{e}\kappa \mathbf{R}_A = \kappa \boldsymbol{\mu}_A \tag{6.94}$$

where the parameter κ is an overlap factor which indicates what fraction of the charge is actually transferred:

$$\kappa = -\frac{\langle e_\epsilon(t_{2g})|\mathcal{H}|\psi^A\rangle}{E_\psi - E_{t_{2g}}} = -\frac{\sqrt{2}H_\pi}{E_\psi - E_{t_{2g}}} \tag{6.95}$$

Note that the transfer term is always polarized in the direction of the transferred charge.

This parametrization can now be used to calculate the transfer term for the relevant trigonal transitions. The Hamiltonian operator is of course totally symmetric, so allowed interactions can take place only between orbitals with the same symmetry, and are independent of the component; hence:

$$\begin{aligned} \left\langle e_\epsilon(t_{2g})|\mathcal{H}|e_\epsilon(\psi)\right\rangle &= \sqrt{3}H_\pi \\ \left\langle e_\theta(t_{2g})|\mathcal{H}|e_\theta(\psi)\right\rangle &= \sqrt{3}H_\pi \end{aligned} \tag{6.96}$$

Symmetry prevents interaction between the $a_1(t_{2g})$ and $a_2(\psi)$ orbitals. The metal-ligand π acceptor interaction will thus stabilize the e-component of the t_{2g} shell, while leaving the a_1-orbital in place, as shown in the simple orbital-energy diagram in the left panel of Fig. 6.6. We can now calculate the transfer term for the $e \rightarrow e$ and $e \rightarrow a_2$ orbital transitions. In each case only one component needs to be calculated. The interaction element in this case is obtained from Eq. (6.96) and the transfer fraction reads:

$$-\frac{\sqrt{3}H_\pi}{E_\psi - E_{t_{2g}}} = \sqrt{\frac{3}{2}}\kappa \tag{6.97}$$

The transfer-dipole element is given by:

$$\frac{1}{6}\left\langle 2\psi^A - \psi^B - \psi^C|\boldsymbol{\mu}|2\psi^A - \psi^B - \psi^C\right\rangle = \frac{1}{6}[4\boldsymbol{\mu}_A + \boldsymbol{\mu}_B + \boldsymbol{\mu}_C] = \frac{1}{2}\boldsymbol{\mu}_A \tag{6.98}$$

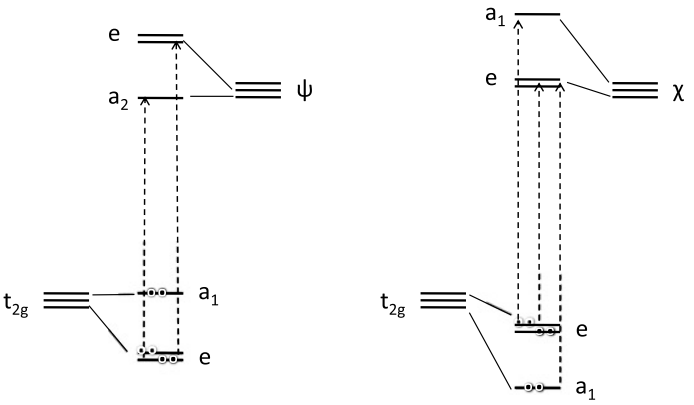

Fig. 6.6 Allowed CT transitions from the t_{2g} shell to ψ- or χ-type ligand acceptor orbitals for tris-chelate complexes with D_3 symmetry

Here, we have made use of the fact that the sum of the three dipole vectors vanishes. The effective transfer term thus becomes:

$$\boldsymbol{\mu}\big(e_\epsilon(t_{2g}) \rightarrow e_\epsilon(\psi)\big) = \sqrt{\frac{3}{8}}\kappa\boldsymbol{\mu}_A \tag{6.99}$$

In the Wigner–Eckart formalism, this matrix element is written as:

$$\big\langle e_\epsilon(t_{2g})|\mu_{x'}|e_\epsilon(\psi)\big\rangle = \langle E\epsilon|E\theta E\epsilon\rangle\big\langle e(t_{2g}) \parallel e(\mu) \parallel e(\psi)\big\rangle \tag{6.100}$$

The coupling coefficient in this equation is equal to $1/\sqrt{2}$. We can thus identify the reduced matrix element as:

$$\big\langle e(t_{2g}) \parallel e(\mu) \parallel e(\psi)\big\rangle = \frac{\sqrt{3}}{2}\kappa\mu_A \tag{6.101}$$

All other $e \rightarrow e$ transfer terms can then be obtained by simply varying the coupling coefficients. We give one more example of a transition that requires an operator which is $\mu_{y'}$ polarized:

$$\begin{aligned}\big\langle e_\theta(t_{2g})|\boldsymbol{\mu}|e_\epsilon(\psi)\big\rangle &= \frac{1}{\sqrt{8}}\kappa\big\langle\psi^C - \psi^B|\boldsymbol{\mu}|2\psi^A - \psi^B - \psi^C\big\rangle \\ &= \frac{1}{\sqrt{8}}\kappa(\boldsymbol{\mu}_B - \boldsymbol{\mu}_C)\end{aligned} \tag{6.102}$$

The vector $\boldsymbol{\mu}_B - \boldsymbol{\mu}_C$ in this expression is directed in the $\mu_{y'}$ direction, as required by the selection rule. Moreover, the length of this vector is $\sqrt{3}\mu^\perp$:

$$(\boldsymbol{\mu}_B - \boldsymbol{\mu}_C)\cdot(\boldsymbol{\mu}_B - \boldsymbol{\mu}_C) = 2\big(\mu^\perp\big)^2 - 2\boldsymbol{\mu}_B\cdot\boldsymbol{\mu}_C = 3\big(\mu^\perp\big)^2 \tag{6.103}$$

Hence, the transfer-dipole length for this y'-polarized transition also measures $\sqrt{3/8}\kappa$, which is exactly the same as for the x'-polarized transition, given in Eq. (6.99). This is expected since the corresponding coupling coefficients, $\langle E\epsilon|E\theta E\epsilon\rangle$ and $\langle E\theta|E\epsilon E\epsilon\rangle$, are equal.

Using the transfer model, we can also express the reduced matrix elements for the $e \to a_2$ channel. Even though there is no overlap between these orbitals, they do give rise to a transfer-term intensity. Orbital interaction does indeed delocalize the $e(t_{2g})$ orbitals over the ligands. The dipole operators, centred on the complex origin, will then couple the $e(\psi)$ and $a_2(\psi)$ ligand-centred orbitals. Hence, we write:

$$\begin{aligned}\boldsymbol{\mu}\big(e_\epsilon(t_{2g}) \to a_2(\psi)\big) &= -\frac{\langle e_\epsilon(t_{2g})|\mathcal{H}|e_\epsilon(\psi)\rangle}{E_\psi - E_{t_{2g}}}\big\langle e_\epsilon(\psi)|\boldsymbol{\mu}|a_2(\psi)\big\rangle \\ &= \sqrt{\frac{3}{2}}\kappa\big\langle e_\epsilon(\psi)|\boldsymbol{\mu}|a_2(\psi)\big\rangle \end{aligned} \tag{6.104}$$

The dipole matrix element in this expression can easily be evaluated:

$$\begin{aligned}\big\langle e_\epsilon(\psi)|\boldsymbol{\mu}|a_2(\psi)\big\rangle &= \frac{1}{3\sqrt{2}}\big\langle 2\psi^A - \psi^B - \psi^C|\boldsymbol{\mu}|\psi^A + \psi^B + \psi^C\big\rangle \\ &= \frac{1}{3\sqrt{2}}(2\boldsymbol{\mu}_A - \boldsymbol{\mu}_B - \boldsymbol{\mu}_C) \\ &= \frac{1}{\sqrt{2}}\boldsymbol{\mu}_A \end{aligned} \tag{6.105}$$

The total transfer term is obtained by combining Eqs. (6.104) and (6.105):

$$\boldsymbol{\mu}\big(e_\epsilon(t_{2g}) \to a_2(\psi)\big) = \frac{\sqrt{3}}{2}\kappa\boldsymbol{\mu}_A \tag{6.106}$$

A final task is to calculate the transition-moments between the corresponding multi-electronic states based on the orbital-transition moments obtained. In the tris-chelate complex under consideration, a ${}^1A_1 \to {}^1E$ state transition can be associated with each allowed orbital-transition. The ${}^1A_1$ corresponds to the closed-shell ground state, based on the $(t_{2g})^6$ configuration. Both the $e \to a_2$ and $e \to e$ transitions will give rise to a twofold-degenerate ${}^1E$ state. As an example, the θ states are written in determinantal notation as follows, where we write only the orbitals that are singly occupied:

$$\begin{aligned}\big|{}^1E_\theta(e \to a_2)\big\rangle &= \frac{1}{\sqrt{2}}\big[\big|\big(e_\epsilon(t_{2g})\alpha\big)\big(a_2(\psi)\beta\big)\big| - \big|\big(e_\epsilon(t_{2g})\beta\big)\big(a_2(\psi)\alpha\big)\big|\big] \\ \big|{}^1E_\theta(e \to e)\big\rangle &= \frac{1}{2}\big[\big|\big(e_\theta(t_{2g})\alpha\big)\big(e_\theta(\psi)\beta\big)\big| - \big|\big(e_\theta(t_{2g})\beta\big)\big(e_\theta(\psi)\alpha\big)\big| \\ &\quad - \big|\big(e_\epsilon(t_{2g})\alpha\big)\big(e_\epsilon(\psi)\beta\big)\big| + \big|\big(e_\epsilon(t_{2g})\beta\big)\big(e_\epsilon(\psi)\alpha\big)\big|\big] \end{aligned} \tag{6.107}$$

Table 6.5 Transfer-term contributions to ${}^1A_1 \rightarrow {}^1E$ CT transitions, with ψ and χ acceptor orbitals

ψ ligand orbitals		χ ligand orbitals	
${}^1E(a_1 \rightarrow e(\psi))$	0	${}^1E(a_1 \rightarrow e(\chi))$	$\sqrt{2}\kappa'$
${}^1E(e \rightarrow a_2(\psi))$	$\sqrt{\frac{3}{2}}\kappa$	${}^1E(e \rightarrow a_1(\chi))$	$\frac{1}{\sqrt{2}}\kappa'$
${}^1E(e \rightarrow e(\psi))$	$\sqrt{\frac{3}{2}}\kappa$	${}^1E(e \rightarrow e(\chi))$	$\frac{1}{\sqrt{2}}\kappa'$

The resulting state transition-moments are then expressed in terms of orbital transition-moments as:

$$\begin{aligned} \left\langle {}^1A_1|\boldsymbol{\mu}|{}^1E_\theta(e \rightarrow a_2)\right\rangle &= \sqrt{2}\left\langle e_\epsilon(t_2g)|\boldsymbol{\mu}|a_2(\psi)\right\rangle = \sqrt{3/2}\kappa \\ \left\langle {}^1A_1|\boldsymbol{\mu}|{}^1E_\theta(e \rightarrow e)\right\rangle &= 2\left\langle e_\theta(t_2g)|\boldsymbol{\mu}|e_\theta(\psi)\right\rangle = \sqrt{3/2}\kappa \end{aligned} \tag{6.108}$$

On the other hand, the $a_1(t_{2g})$ orbital does not delocalize over the ligands. As a result, there can be no transfer term associated with transitions from this orbital. One expects only a weak contact term. The lowest transition corresponds to $a_1(t_{2g}) \rightarrow a_2(\psi)$. The only non-zero coupling coefficient for this transition is $\langle A_1|A_2A_2\rangle$. This transition will thus be dipole allowed under $\mu_{z'}$. Polarized absorption spectra are in line with this analysis: the spectral onset of the CT region is characterized by a weak absorption band in parallel polarization, followed by two strong absorption bands in perpendicular polarization. This assignment is based on the assumption that the vertical Franck–Condon excitations reach delocalized charge-transfer states. At least in the case of $Ru(bipy)_3^{2+}$, this is supported by detailed spectral measurements [18]. An entirely similar analysis can be performed in the case when the ligand orbital is of χ-type. The transition-moments are collected in Table 6.5. In this case, the ligand and metal part both transform as $a_1 + e$ (see Table 6.4). As a result, three transitions are found to carry transfer-term intensity, as indicated in Fig. 6.6.

Circular Dichroism

The tris-chelate compounds are chiral compounds, with an apparent helical structure, which can easily be related to their circular-dichroic properties by use of symmetry selection rules. The CT transitions that we have just discussed cannot be responsible for the primary CD strength, since they are in-plane polarized, and thus do not carry intrinsic helicity. Instead, the prominent peaks in the CD spectrum are observed at higher energies, and are associated with the intra-ligand $\pi\pi^*$-transitions. These transitions take place between occupied and virtual ligand-centred orbitals which are of opposite signature, and hence are of type $\psi \rightarrow \chi$ or vice-versa. Such transitions are long-axis polarized, i.e. the transition dipole moment is oriented along the ligand bridge as shown in Fig. 6.7.

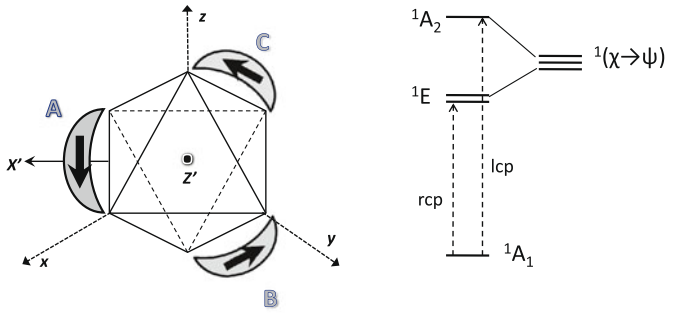

Fig. 6.7 Allowed intra-ligand transitions from χ- to ψ-type ligand orbitals for tris-chelate complexes with D_3 symmetry. The circular dichroism has a lower right-circularly polarized (rcp) band and an upper left-circularly polarized (lcp) band. This gives the CD spectrum the appearance of the first derivative of a Gaussian curve, with a negative part at longer wavelength and a positive part at shorter wavelength

We designate these dipole moments as $\boldsymbol{\mu}_A^{\parallel}, \boldsymbol{\mu}_B^{\parallel}, \boldsymbol{\mu}_C^{\parallel}$. These vectors can be expressed in a row notation for the primed x', y', z' coordinate system as follows:

$$\begin{aligned}
\boldsymbol{\mu}_A^{\parallel} &= \mu^{\parallel}\left(0, \frac{1}{\sqrt{3}}, \frac{\sqrt{2}}{\sqrt{3}}\right) \\
\boldsymbol{\mu}_B^{\parallel} &= \mu^{\parallel}\left(-\frac{1}{2}, -\frac{1}{2\sqrt{3}}, \frac{\sqrt{2}}{\sqrt{3}}\right) \\
\boldsymbol{\mu}_C^{\parallel} &= \mu^{\parallel}\left(\frac{1}{2}, -\frac{1}{2\sqrt{3}}, \frac{\sqrt{2}}{\sqrt{3}}\right)
\end{aligned} \tag{6.109}$$

The scalar products between these orientations are equal to $1/2$, which corresponds to angles of 60°. Each of the three transitions gives rise to an excited state. In D_3 symmetry these states transform as $A_2 + E$. The composition of these *exciton* states[8] is as follows:

$$\begin{aligned}
\left|{}^1A_2\right\rangle &= \frac{1}{\sqrt{3}}\left[(\chi_A \rightarrow \psi_A)^1 + (\chi_B \rightarrow \psi_B)^1 + (\chi_C \rightarrow \psi_C)^1\right] \\
\left|{}^1E_\theta\right\rangle &= \frac{1}{\sqrt{2}}\left[-(\chi_B \rightarrow \psi_B)^1 + (\chi_C \rightarrow \psi_C)^1\right] \\
\left|{}^1E_\epsilon\right\rangle &= \frac{1}{\sqrt{6}}\left[2(\chi_A \rightarrow \psi_A)^1 - (\chi_B \rightarrow \psi_B)^1 - (\chi_C \rightarrow \psi_C)^1\right]
\end{aligned} \tag{6.110}$$

[8]The excitation creates an electron-hole pair, which can move from one ligand to another. This is called an exciton.

Here, the notation refers to a singlet orbital transition, which can be written in determinantal form as:

$$(\chi_A \to \psi_A)^1 = \frac{1}{\sqrt{2}}\big[\big|(\chi_A\alpha)(\psi_A\beta)\big| - \big|(\chi_A\beta)(\psi_A\alpha)\big|\big] \tag{6.111}$$

To first approximation, the metal centre is not taking part in the electronic properties, but merely serves as a structural template which keeps the ligands in place. Distant interactions between the three transitions can be described by a simple exciton-coupling model. In this model, the interaction between transitions is approximated by the electrostatic interaction potential between the corresponding transition dipoles. This potential is given by:

$$V_{ij} = \frac{1}{4\pi\epsilon_0}\left(\frac{\boldsymbol{\mu}^i \cdot \boldsymbol{\mu}^j}{R_{ij}^3} - \frac{3(\boldsymbol{\mu}^i \cdot \mathbf{R}_{ij})(\boldsymbol{\mu}^j \cdot \mathbf{R}_{ij})}{R_{ij}^5}\right) \tag{6.112}$$

where R_{ij} is the distance between the dipoles, and $\mathbf{R}_{ij} = \mathbf{R}_j - \mathbf{R}_i$. The length of the distance vector is thus $\sqrt{3}\rho$. The energies of the exciton states are then given by:

$$\begin{aligned} \big\langle {}^1A_2|V|{}^1A_2\big\rangle &= \frac{(\mu^{\parallel})^2}{4\pi\epsilon_0\rho^3}\frac{1}{6\sqrt{3}} \\ \big\langle {}^1E|V|{}^1E\big\rangle &= -\frac{(\mu^{\parallel})^2}{4\pi\epsilon_0\sqrt{3}\rho^3}\frac{1}{12\sqrt{3}} \end{aligned} \tag{6.113}$$

The ${}^1A_2$ state thus goes up in energy twice as much as the ${}^1E$ state goes down, thus keeping the barycentre energy at the zeroth-order position. Now, in order to determine the CD strength, we need for the two states both the electric and the magnetic transition dipoles from the ground state. The electric dipoles are easily obtained by combining the state vectors:

$$\begin{aligned} \boldsymbol{\mu}\big({}^1A_1 \to {}^1A_2\big) &= \frac{1}{\sqrt{3}}\big(\boldsymbol{\mu}_A^{\parallel} + \boldsymbol{\mu}_B^{\parallel} + \boldsymbol{\mu}_C^{\parallel}\big) = \sqrt{2}\mu^{\parallel}(0,0,1) \\ \boldsymbol{\mu}\big({}^1A_1 \to {}^1E_{\epsilon}\big) &= \frac{1}{\sqrt{6}}\big(2\boldsymbol{\mu}_A^{\parallel} - \boldsymbol{\mu}_B^{\parallel} - \boldsymbol{\mu}_C^{\parallel}\big) = \frac{1}{\sqrt{2}}\mu^{\parallel}(0,1,0) \\ \boldsymbol{\mu}\big({}^1A_1 \to {}^1E_{\theta}\big) &= \frac{1}{\sqrt{2}}\big(-\boldsymbol{\mu}_B^{\parallel} + \boldsymbol{\mu}_C^{\parallel}\big) = \frac{1}{\sqrt{2}}\mu^{\parallel}(1,0,0) \end{aligned} \tag{6.114}$$

The calculation of the magnetic transition dipoles requires a preamble. The magnetic moment was already defined in Eq. (4.128) of Chap. 4. By explicitly writing the angular momentum operator in terms of the linear momentum operator as $\boldsymbol{r} \times \boldsymbol{p}$ one obtains:

$$\boldsymbol{m} = -\frac{\mathrm{e}}{2m}\boldsymbol{l} = -\frac{\mathrm{e}}{2m}\boldsymbol{r} \times \boldsymbol{p} \tag{6.115}$$

The commutator of the one-electron Hamiltonian with the position operator is given by:

$$[\mathcal{H}, \boldsymbol{r}] = \left[\left(\frac{\boldsymbol{p}\cdot\boldsymbol{p}}{2m} + V(\boldsymbol{r})\right), \boldsymbol{r}\right] = -\frac{i\hbar}{m}\boldsymbol{p} \tag{6.116}$$

Here, we used the Heisenberg commutator relation between the conjugate position and momentum operators: $[x, p_x] = i\hbar$. The magnetic moment matrix element of the intra-ligand transition with respect to the common origin of the coordinate system is given by:

$$\mathbf{m}_A = \langle\psi_A|\boldsymbol{m}|\chi_A\rangle = -\frac{\mathrm{e}}{2m}\big\langle\psi_A|(\mathbf{R}_A + \boldsymbol{r}) \times \boldsymbol{p}|\chi_A\big\rangle = -\frac{\mathrm{e}}{2m}\mathbf{R}_A \times \langle\psi_A|\boldsymbol{p}|\chi_A\rangle \tag{6.117}$$

where it was assumed that the chromophore has no intrinsic magnetic transition-moment. The momentum matrix element in this equation can now be evaluated with the help of Eq. (6.116):

$$\begin{aligned}\langle\psi_A|\boldsymbol{p}|\chi_A\rangle &= \frac{im}{\hbar}\langle\psi_A|\mathcal{H}\boldsymbol{r} - \boldsymbol{r}\mathcal{H}|\chi_A\rangle \\ &= \frac{im}{\hbar}\big(\langle\mathcal{H}\psi_A|\boldsymbol{r}|\chi_A\rangle - \langle\psi_A|\boldsymbol{r}\mathcal{H}|\chi_A\rangle\big) \\ &= \frac{im}{\hbar}(E_\psi - E_\chi)\langle\psi_A|\boldsymbol{r}|\chi_A\rangle \\ &= 2\pi i m\nu\langle\psi_A|\boldsymbol{r}|\chi_A\rangle\end{aligned} \tag{6.118}$$

Here, ν is the frequency of the intra-ligand transition. The combination of this result with Eq. (6.117) yields:

$$\begin{aligned}\mathbf{m}_A &= i\pi\nu\big(\mathbf{R}_A \times \boldsymbol{\mu}_A^{\parallel}\big) = i\pi\nu\rho\mu^{\parallel}\left(0, -\frac{\sqrt{2}}{\sqrt{3}}, \frac{1}{\sqrt{3}}\right) \\ \mathbf{m}_B &= i\pi\nu\big(\mathbf{R}_B \times \boldsymbol{\mu}_B^{\parallel}\big) = i\pi\nu\rho\mu^{\parallel}\left(\frac{1}{\sqrt{2}}, \frac{1}{\sqrt{6}}, \frac{1}{\sqrt{3}}\right) \\ \mathbf{m}_C &= i\pi\nu\big(\mathbf{R}_C \times \boldsymbol{\mu}_C^{\parallel}\big) = i\pi\nu\rho\mu^{\parallel}\left(-\frac{1}{\sqrt{2}}, \frac{1}{\sqrt{6}}, \frac{1}{\sqrt{3}}\right)\end{aligned} \tag{6.119}$$

As we indicated the above formalism applies to chromophores that have no intrinsic magnetic moment.

$$\begin{aligned}\mathbf{m}\big({}^1A_1 \to {}^1A_2\big) &= \frac{1}{\sqrt{3}}\big(\mathbf{m}_A^{\parallel} + \mathbf{m}_B^{\parallel} + \mathbf{m}_C^{\parallel}\big) = i\pi\nu\rho\mu^{\parallel}(0, 0, 1) \\ \mathbf{m}\big({}^1A_1 \to {}^1E_\epsilon\big) &= \frac{1}{\sqrt{6}}\big(2\mathbf{m}_A^{\parallel} - \mathbf{m}_B^{\parallel} - \mathbf{m}_C^{\parallel}\big) = -i\pi\nu\rho\mu^{\parallel}(0, 1, 0) \\ \mathbf{m}\big({}^1A_1 \to {}^1E_\theta\big) &= \frac{1}{\sqrt{2}}\big(-\mathbf{m}_B^{\parallel} + \mathbf{m}_C^{\parallel}\big) = -i\pi\nu\rho\mu^{\parallel}(1, 0, 0)\end{aligned} \tag{6.120}$$

A transition will be characterized by a helical displacement of the electron if the magnetic and electric transition dipoles are aligned. This is reflected in the Rosenfeld equation for the CD intensity or *rotatory strength*, $\mathcal{R}_{a\to j}$, for a transition from a ground state a to an excited state j in a collection of randomly-oriented molecules:

$$\mathcal{R}_{a\to j} = \mathrm{Im}\big\{\langle a|\boldsymbol{\mu}|j\rangle \cdot \langle j|\boldsymbol{m}|a\rangle\big\} \tag{6.121}$$

Straightforward application to the exciton bands yields:

$$\begin{aligned}
\mathcal{R}\big({}^1A_1 \to {}^1A_2\big) &= \sqrt{2}\pi\nu\rho\big(\mu^{\parallel}\big)^2 \\
\mathcal{R}\big({}^1A_1 \to {}^1E_{\epsilon}\big) &= -\frac{1}{\sqrt{2}}\pi\nu\rho\big(\mu^{\parallel}\big)^2 \\
\mathcal{R}\big({}^1A_1 \to {}^1E_{\theta}\big) &= -\frac{1}{\sqrt{2}}\pi\nu\rho\big(\mu^{\parallel}\big)^2
\end{aligned} \tag{6.122}$$

The out-of-plane polarized transition to the ${}^1A_2$ state, which lies at higher energy, has a positive CD signal, while the in-plane polarized transition to the lower ${}^1E$ state has a negative CD signal. The latter transition consists of two components along the two in-plane directions. Summing over the three components in Eq. (6.122), shows that the total rotatory strength, for randomly-oriented molecules, is exactly zero. This is a general sum rule for CD spectra. If one now takes the spectrum of the chiral antipode, the Λ tris-chelate complex, the spectra are exactly the same but the signs are reversed. Mirror image in actual geometry thus becomes reflection symmetry in the spectrum.

6.9 Induction Revisited: The Fibre Bundle

In Chap. 4 we left induction after the proof of the Frobenius reciprocity theorem. In that proof the important concept of the positional representation was introduced. This described the permutation of the sites under the action of the group elements. Further, we defined local functions on the sites which transformed as irreps of the site symmetry. As an example, if we want to describe the displacement of a cluster atom in a polyhedron, two local functions are required: a totally-symmetric one for the radial displacement and a twofold-degenerate one for the tangential displacements. In cylindrical symmetry, these are labelled σ and π, respectively. The *mechanical* representation, i.e. the representation of the cluster displacements, is then the sum of the two induced representations:

$$\Gamma_{\mathrm{mech}} = \Gamma(\sigma H \uparrow G) + \Gamma(\pi H \uparrow G) \tag{6.123}$$

As an example using the induction tables in Sect. C.2 for an octahedron, we have:

$$\Gamma_{\mathrm{mech}} = (A_{1g} + E_g + T_{1u}) + (T_{1g} + T_{2g} + T_{1u} + T_{2u}) \tag{6.124}$$

This is precisely the set of fluorine displacements that we constructed in Sect. 4.8 in order to describe the vibrational modes of UF_6. One remarkable result of induction theory is that the mechanical representation can also be obtained as the direct product of the positional representation and the translational representation, T_{1u}; this is the representation of the three displacements of the centre of the cluster.

$$\begin{aligned}\Gamma_{\text{mech}} &= T_{1u} \times (A_{1g} + E_g + T_{1u}) \\ &= T_{1u} + (T_{1u} + T_{2u}) + (A_{1g} + E_g + T_{1g} + T_{2g})\end{aligned} \tag{6.125}$$

It is as if the displacements of the central point of the octahedron were relocated to every ligand site. The elementary function space of the displacements of the central atom, which transforms as the translational irrep, T_{1u}, is called the *standard fibre*. This fibre is attached to every site of the cluster, and the set of these fibres is the *fibre bundle*. The action of the group permutes fibres of the bundle. The following induction theorem holds:

Theorem 14 *Consider a standard fibre, consisting of a function space that is invariant under the action of the group. In a cluster of equivalent sites, we can form a fibre bundle by associating this standard fibre with every site position. The induced representation of the fibre bundle is then the direct product of the irrep of the standard fibre with the positional representation.*

For $\mathcal{V}$ being the representation of the standard fibre, T_{1u} in our example, and $\mathcal{P}$ the positional representation of the set of equivalent sites in the molecule, one has for the induced representation:

$$\Gamma\big(\{\mathcal{V}\}H \uparrow G\big) = \mathcal{V} \times \mathcal{P}(H \uparrow G) \tag{6.126}$$

For a proof of this theorem, we refer to the literature [19, 20]. The theorem is not only applicable to molecular vibrations but is also directly in line with the LCAO method in molecular quantum chemistry. In this method the molecular orbitals (MOs) are constructed from atomic basis sets that are defined on the constituent atoms. An atomic basis set, such as $3d$ or $4f$, corresponds to a fibre, emanating, as it were, from the atomic centre. Usually, such basis sets obey spherical symmetry, since they are defined for the isolated atoms. As such, they are also invariant under the molecular point group [21]. As an example, a set of $4f$ polarisation functions on a chlorine ligand in a $RhCl_6^{3-}$ complex is itself adapted to octahedral symmetry as $a_{2u} + t_{1u} + t_{2u}$. This representation thus corresponds to $\mathcal{V}$. In the C_{4v} site symmetry these irreps subduce: $a_1 + b_1 + b_2 + 2e$. According to the theorem, the LCAOs based on the $4f$ orbitals thus will transform as:

$$\begin{aligned}&\Gamma\big(\{a_1 + b_1 + b_2 + 2e\}C_{4v} \uparrow O_h\big) \\ &= (a_{2u} + t_{1u} + t_{2u}) \times (a_{1g} + e_g + t_{1u}) \\ &= a_{1g} + a_{2g} + 2e_g + 2t_{1g} + 3t_{2g} + a_{2u} + e_u + 3t_{1u} + 3t_{2u}\end{aligned} \tag{6.127}$$

In this LCAO space several irreps occur multiple times, but they can all be distinguished by the specific direct product from which they originated.

6.10 Application: Bonding Schemes for Polyhedra

Leonhard Euler dominated the mathematics of the 18th century. One of his famous discoveries was the polyhedral theorem, which marks the beginning of topology. A polyhedron has three structural elements: vertices, edges, and faces.[9] The numbers of these will be represented as v, e, and f, respectively. Then, for a polyhedron, the following theorem holds:

Theorem 15 *In a convex polyhedron the alternating sum of the numbers of vertices, edges, and faces is always equal to* 2.

$$v - e + f = 2 \tag{6.128}$$

As an example, in a cube one has $v = 8$, $e = 12$, $f = 6$, and hence $8 - 12 + 6 = 2$. The 2 in the right-hand side of Eq. (6.128) is called the Euler invariant. It is a *topological* characteristic. Topology draws attention to properties of surfaces, which are not affected when surfaces are stretched or deformed, as one can do with objects made of rubber or clay. Topology is thus not concerned with regular shapes, and in this sense seems to be completely outside our subject of symmetry; yet, as we intend to show in this section, there is in fact a deep connection, which also carries over to molecular properties. The surface to which the 2 in the theorem refers is the surface of a sphere. A convex polyhedron is indeed a polyhedron which can be embedded or mapped on the surface of a sphere. Group theory, and in particular the induction of representations, provides the tools to understand this invariant. To this end, each of the terms in the Euler equation is replaced by an induced representation, which is based on the particular nature of the corresponding structural element. In Fig. 6.8 we illustrate the results for the case of the tetrahedron.

- The vertices, being zero-dimensional points, form a set of nodes, $\{\langle u \rangle\}$, which are permuted under the symmetry operations of the polyhedron. The representation of this set is the positional representation, $\Gamma_\sigma(v)$. The σ here refers to the fact that the sites themselves transform as totally-symmetric objects in the site group. If the cluster contains several orbits, the induced representation is of course the sum of the individual positional representations. In Fig. 6.8 the vertex representation is $A_1 + T_2$. In Sect. 4.7 we have already encountered these irreps, when discussing the sp^3 hybridization of carbon.

$$\Gamma_\sigma(v) = \Gamma(a_1 C_{3v} \uparrow T_d) = A_1 + T_2 \tag{6.129}$$

[9] In geometry a *vertex* is a point were two or more lines meet.

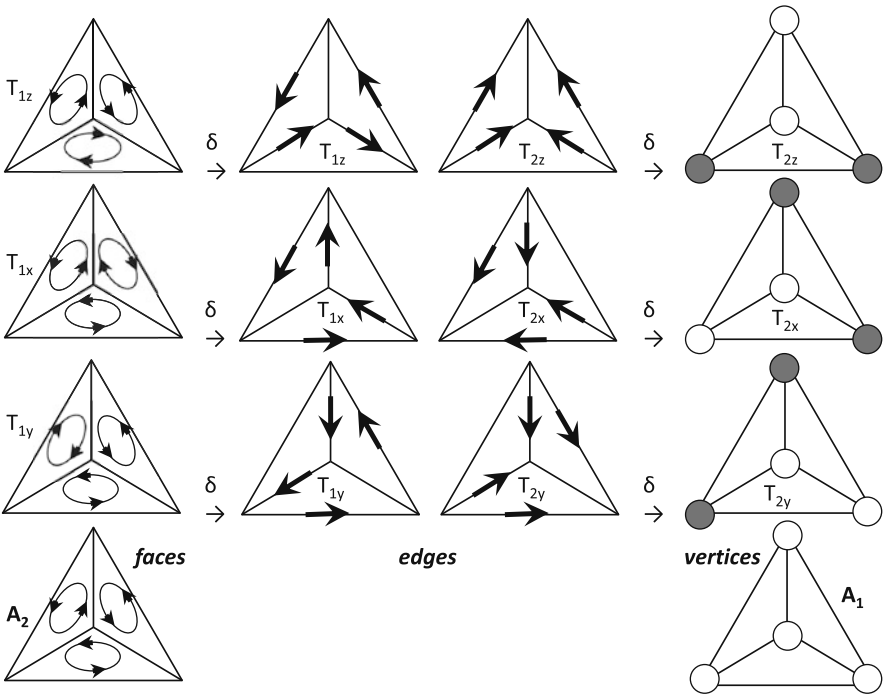

Fig. 6.8 Face, edge and vertex SALCs for a tetrahedron. The δ symbol denotes taking the boundary, from faces to edges, and from edges to vertices (see text). The two topological invariants are the A_2 face term and the A_1 vertex term

- The edges are one-dimensional lines. They form a set of ordered pairs, $\{\langle u, v\rangle\}$. Each of these can be thought of as an arrow, directed along the edge. The symmetry operations will interchange these arrows, but may also change their sense. The corresponding representation is labelled as $\Gamma_{\parallel}(e)$. This symbol indicates that the basic objects on the edge sites are not symmetric points but directed arrows. The site group through the centre of an edge has maximal symmetry C_{2v} and in this site group the arrows transform as the b_1 irrep, which is symmetric under reflection in a plane containing the edge and antisymmetric under the symmetry plane perpendicular to the edge. For a tetrahedron there are six edge vectors, transforming as $T_1 + T_2$.

$$\Gamma_{\parallel}(e) = \Gamma(b_1 C_{2v} \uparrow T_d) = T_1 + T_2 \tag{6.130}$$

- The faces may be represented as closed chains of nodes, which are bordering a polyhedral face, $\{\langle u, v, w, \ldots\rangle\}$. The sequence forms a circulation around the face, in a particular sense (going from $\langle u\rangle$ to $\langle w\rangle$ over $\langle v\rangle$, etc.). The set of face rotations forms the basis for the face representation, which is denoted as $\Gamma_{\circlearrowleft}(f)$. In a polyhedron the maximal site group of a face is C_{nv}, and in this site group the face rotation transforms as the rotation around the $\hat{C}_n$ axis, i.e. it is symmetric

under the axis and antisymmetric with respect to the vertical $\hat{\sigma}_v$ planes, which invert the sense of rotation. For the tetrahedron, the face circulations transform as $A_2 + T_2$, as shown in Fig. 6.8.

$$\Gamma_{\circlearrowleft} = \Gamma(a_2 C_{3v} \uparrow T_d) = A_2 + T_1 \tag{6.131}$$

The following theorem [22] applies:

Theorem 16 *The alternating sum of induced representations of the vertex nodes, edge arrows, and face rotations, is equal to the sum of the totally-symmetric representation, Γ_0, and the pseudo-scalar representation, Γ_ϵ. The latter representation is symmetric under proper symmetry elements and antisymmetric under improper symmetry elements.*

$$\Gamma_\sigma(v) - \Gamma_\parallel(e) + \Gamma_{\circlearrowleft}(f) = \Gamma_0 + \Gamma_\epsilon \tag{6.132}$$

The Euler theorem may be considered as the dimensional form of this theorem, which states that the alternating sum of the characters of the induced representations under the unit element, $\hat{E}$, is equal to 2, but the present theorem extends this character equality to all the operations of the group. The theorem silently implies that irreps can be added and subtracted. In the example of the tetrahedron, the theorem is expressed as:

$$\Gamma_\sigma(v) - \Gamma_\parallel(e) + \Gamma_{\circlearrowleft}(f) = (A_1 + T_2) - (T_1 + T_2) + (A_2 + T_2) = A_1 + A_2 \tag{6.133}$$

A straightforward interpretation of the theorem is possible in terms of fluid flow on the surface of a polyhedron.[10] Suppose observers are positioned on the vertices, edge centres and face centres, and register the local fluid flow. When the incoming and outgoing currents at a node are not in balance, the observers located on these nodes will report piling up or depletion of the local fluid level. This is the scalar property represented by the vertex term. The corresponding connection between edge flow and vertex density is expressed by the *boundary operation*, indicated by δ in Fig. 6.8. Taking the boundary of an edge arrow means replacing the arrow by the difference of two vertex-localized scalars: a positive one (indicated by a white circle in the figure) at the node to which the arrow's head is pointing, and a negative one (indicated by a black circle) at the node facing the arrow's tail. This projection from edge to vertex will not change the symmetry. Hence, in this way, the boundary of the T_2 edge irrep is the T_2 vertex SALC, as illustrated in the figure. Similarly, observers in face centres will notice the net current that is circulating around the face. Such a circular current through the edges does not give rise to changes at the nodes (indeed the incoming flow at a node is also leaving again), but is observable from the centre of the face around which the current is circulating. The boundaries

[10]This flow description provides a simple pictorial illustration of the abstract homology theory. The standard reference is: [23].

of circular currents around face centres are thus chains of arrows on the edges, which again conserve the symmetry. In Fig. 6.8 the boundary of the T_1 face term is thus the T_1 edge term. Clearly, the sum of the vertex and face observations should account for all currents going through the edges, except for two additional terms which escape edge observations. These are the two Euler invariants: the totally-symmetric Γ_0 component corresponds to a uniform change of fluid amplitude at all vertex basins. This does not give rise to edge currents, since it creates no gradients over the edges. The other is the Γ_ϵ component. It corresponds to a simultaneous rotation around all faces in the same sense. Again, such rotor flows do not create net flows through the edges, because two opposite currents are flowing through every edge. The Euler invariant thus points to two invariant characteristic modes of the sphere. They are not boundaries of a mode at a higher level, nor are they bounded by a mode at a lower level. The phenomena, that these two terms describe, might also be referred to in a topological context as the electric and magnetic *monopoles*.

Because of this connection to density and current, this theorem may be applied in various ways to describe chemical bonding, frontier orbital structure, and vibrational properties. The applications of this theorem can be greatly extended by introducing fibre representations, as is shown below.

Taking the Dual To take the dual of a polyhedron is to replace vertices by faces and vice-versa, as was already mentioned in Sect. 3.7 in relation to the Platonic solids. The dual has the same number of edges as the original, but every edge is rotated 90°. Hence the relations between v^D, e^D, f^D for the dual and v, e, f for the original are:

$$\begin{aligned} v^D &= f \\ e^D &= e \\ f^D &= v \end{aligned} \tag{6.134}$$

As a result the Euler formula is invariant under the dual operation.

$$v - e + f = v^D - e^D + f^D = 2 \tag{6.135}$$

A similar invariance holds for the symmetry extension, but in this case "to take the dual" corresponds to multiplying all terms by the pseudo-scalar irrep Γ_ϵ. The terms are then changed as follows:

$$\begin{aligned} \Gamma_\sigma(v) \times \Gamma_\epsilon &= \Gamma_\circlearrowleft(v) = \Gamma_\circlearrowleft\left(f^D\right) \\ \Gamma_\parallel(e) \times \Gamma_\epsilon &= \Gamma_\perp(e) = \Gamma_\parallel\left(e^D\right) \\ \Gamma_\circlearrowleft(f) \times \Gamma_\epsilon &= \Gamma_\sigma(f) = \Gamma_\sigma\left(v^D\right) \\ (\Gamma_0 + \Gamma_\epsilon) \times \Gamma_\epsilon &= \Gamma_0 + \Gamma_\epsilon \end{aligned} \tag{6.136}$$

Hence, if the theorem holds for the original, it also holds for the dual.

$$\left(\Gamma_\sigma(v) - \Gamma_\parallel(e) + \Gamma_\circlearrowleft(f)\right) \times \Gamma_\epsilon = \Gamma_\sigma\left(v^D\right) - \Gamma_\parallel\left(e^D\right) + \Gamma_\circlearrowleft\left(f^D\right) = \Gamma_0 + \Gamma_\epsilon \tag{6.137}$$

Note especially the fibre modification of the edge term. The maximal local symmetry of an edge is C_{2v}. The arrow along the edge transforms as b_1, while the pseudo-scalar irrep in C_{2v} is a_2. The product $b_1 \times a_2$ produces b_2, which is precisely the symmetry of an arrow, tangent to the surface of the polyhedron, but directed perpendicular to the edge. Multiplication with the pseudo-scalar irrep thus has the effect of rotating the edges through 90°. In Eq. (6.136) the resulting representation is denoted as $\Gamma_\perp(e)$.

Deltahedra Deltahedra are polyhedra that consist entirely of triangular faces. Three of the Platonic solids are deltahedra: the tetrahedron, the octahedron and the icosahedron. In a convex deltahedron the bond stretches (i.e. stretchings of the edges) span precisely the representation of the internal vibrations. In other words, a convex deltahedron cannot vibrate if it is made of rigid rods. This is the Cauchy theorem:

Theorem 17 *Convex polyhedra in three dimensions with congruent corresponding faces must be congruent to each other. In consequence, if a polyhedron is made up of triangles with rigid rods, the angles between the triangular faces are fixed.*

This result can be cast in the language of induced representations. The stretchings of the edges correspond to scalar changes of edge lengths and transform as σ-type objects, and hence will correspond to $\Gamma_\sigma(e)$. On the other hand, the internal vibrations span the mechanical representation, which can be written as a bundle of the translation, minus the spurious modes of translation and rotation. The symmetries of these will be denoted as Γ_T and Γ_R, respectively. One thus has:

$$\text{Deltahedron:} \quad \Gamma_\sigma(v) \times \Gamma_T - \Gamma_T - \Gamma_R = \Gamma_\sigma(e) \tag{6.138}$$

Trivalent Polyhedra The dual of a deltahedron is a trivalent polyhedron, meaning that every vertex is connected to three nearest neighbours. The fullerene networks of carbon are usually trivalent polyhedra. This reflects the sp^2 hybridization of carbon, which can form three σ-bonds. Also in this case several specialized forms of the Euler symmetry theorem can be formulated. We may start from Eq. (6.138) and replace vertices by faces. The edge terms remain the same since they are totally symmetric under the local symmetries of the edges. Rotations of the edges by 90° will thus not affect these terms.

$$\text{Trivalent:} \quad \Gamma_\sigma(f) \times \Gamma_T - \Gamma_T - \Gamma_R = \Gamma_\sigma(e) \tag{6.139}$$

Furthermore, by multiplying the vertices in a trivalent polyhedron by three, we have accounted for all the edges twice, since each edge is linked to two vertices, hence:

$$\text{Trivalent:} \quad 3v = 2e \tag{6.140}$$

The $3v$ in this formula suggests once again taking the fibre representation $\Gamma_\sigma(v) \times \Gamma_T$. In doing so we have considered on each vertex one σ and two π

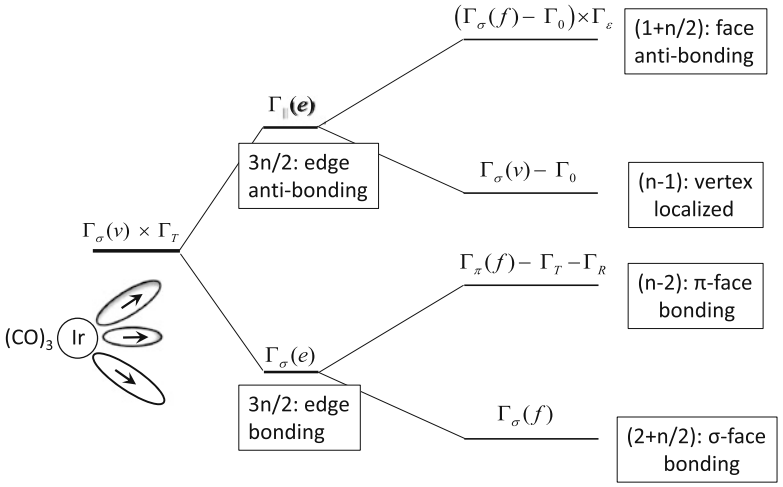

Fig. 6.9 Edge bonding in electron-precise trivalent cages. The valence shell splits into an occupied set of localized edge-bonds, and a matching virtual set of edge-anti-bonds. The sets may be further differentiated by use of the symmetry theorems

objects. Hence, this is not only the mechanical representation with three displacements on each vertex, but it is equally well the symmetry of a set of sp^2 hybrids on every vertex, directed along the three edges. Along each edge the hybrids at either end can be combined in a local bonding and anti-bonding combination. The corresponding induced representations are respectively: $\Gamma_\sigma(e)$ and $\Gamma_\parallel(e)$; hence, the symmetry extension of Eq. (6.140) reads:

$$\text{Trivalent:} \quad \Gamma_\sigma(v) \times \Gamma_T = \Gamma_\sigma(e) + \Gamma_\parallel(e) \tag{6.141}$$

Edge Bonding in Trivalent Polyhedra

The understanding of the bonding schemes in polyhedra is based on the correct identification of the local hybridization scheme on the constituent fragments. Trivalent polyhedra are often *electron-precise*: this means that the fragment has three electrons in three orbitals, which are available for cluster bonding and give rise to edge-localized σ-bonds. Such is the case for the methyne fragment, CH, forming *polyhedranes*, but equally well for the *isolobal* [24] organo-transition-metal fragments such as $M(CO)_3$, where M is a d^9 metal such as Co, Rh or Ir. Figure 6.9 shows the bonding pattern based on such electron-precise fragments. As indicated before, the orbital basis corresponds to the fibre representation $\Gamma_\sigma(v) \times \Gamma_T$, and contains $3n$ orbitals. Local interactions along the edges will split this orbital basis into an occupied σ-bonding half and a virtual σ-anti-bonding counterpart, transforming as $\Gamma_\sigma(e)$ and $\Gamma_\parallel(e)$, respectively. This is precisely the result of Eq. (6.141). Now,

for each half, a more detailed pattern can be discerned [25]. For the anti-bonding orbitals, the general theorem, Eq. (6.132), can be applied directly. The result is illustrated in Fig. 6.9. By this theorem, the $3n/2$ edge anti-bonds are split into two subsets containing $(1 + n/2)$ and $(n - 1)$ orbitals. The former, higher lying, subset transforms as $\Gamma_{\circlearrowleft} - \Gamma_{\epsilon}$. These terms correspond to circulations around the faces, which means that these levels will be highly anti-bonding. In fact, they are always at the top of the skeletal spectrum. Note that the pseudo-scalar term, Γ_{ϵ}, does not take part. This is because a uniform circulation around all faces in the same sense has no contribution on the edges. Below this is a subset of weakly anti-bonding orbitals, transforming as $\Gamma_{\sigma}(v) - \Gamma_0$. These orbitals are more localized on the vertices. The Γ_0 term is not included since this is the totally-symmetric molecular orbital which is completely bonding, and thus will appear in the lower half of the diagram.

Furthermore, the edge-bonding half can be analysed with the help of Eq. (6.139). The $3n/2$ edge bonds split into two subsets of dimension $(n - 2)$ and $(2 + n/2)$. This analysis involves the fibre representation $\Gamma_{\sigma}(f) \times \Gamma_T$, which can be decomposed into a radial σ- and tangential π-part. The σ-part corresponds to cylindrically-symmetric bonds around the faces, and will thus be strongly bonding. For the π-part the face terms contain a nodal plane through the faces, and thus will be less bonding.

Frontier Orbitals in Leapfrog Fullerenes

Fullerenes are trivalent polyhedra of carbon, consisting of hexagons and pentagons. The following relations hold:

$$\begin{aligned} v - e + f &= 2 \\ 3v &= 2e \\ f_5 + f_6 &= f \\ 5f_5 + 6f_6 &= 3v \end{aligned} \tag{6.142}$$

The first two relationships are from Eqs. (6.128) and (6.140). The third expresses that the total number of the faces is the sum of the number of pentagons (f_5), and hexagons (f_6). The final equation indicates that by counting the hexagons six times, and the pentagons five times, we have counted all vertices three times, since every vertex is at the junction of three faces. Even though there are fewer equations, here, than unknowns, it can easily be seen by manipulation of Eq. (6.142) that the only value that the number of pentagons, f_5, can take on is 12. Hence, the smallest fullerene is the dodecahedron C_{20}, which only consists of pentagons. Also note that the number of atoms in a fullerene must be even, since $3v$ must be divisible by 2, as e is an integer. Taking the *leapfrog*, L, of a primitive fullerene, P, is an operation of cage expansion, which yields a fullerene with three times as many atoms [26]. This procedure is described by the following rule:

$$L = \text{Dual}(\text{Omnicap}\, P) \tag{6.143}$$

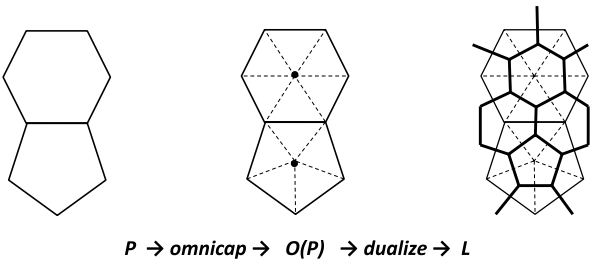

Fig. 6.10 The leapfrog extension consists of two operations: first, place an extra atom in the centres of all the polygons (*middle panel*), then, take the dual. The result is indicated by *the solid lines* in *the right panel*

It involves two operations, which are carried out consecutively, as illustrated in Fig. 6.10. One first places an extra *capping* atom on all pentagons and hexagons. This leads to a cage which consists only of triangles, and this is a deltahedron. By taking the dual one restores a trivalent cage. As can be seen, all vertices of the primitive have been turned into hexagons, while the original pentagons and hexagons are recovered, but in a rotational stagger. The edges of the primitive are also recovered, but rotated 90°. In summary, the leapfrog operation inserts 6 vertices in the hexagons of P, and 5 vertices in the pentagons, which, according to the final expression in Eq. (6.142), multiplies the number of atoms by 3. The first and best known leapfrog is Buckminsterfullerene, C_{60}, which is the leapfrog of the dodecahedron itself. Each carbon atom contributes, besides the sp^2 orbitals, which build the σ-frame, one radial p_r-orbital. These orbitals form π-bonds which control the frontier orbitals of fullerenes. In the case of the leapfrog, this frontier MO region is always characterized by six low-lying almost non-bonding orbitals, which, moreover, always transform as $\Gamma_T + \Gamma_R$. This can be explained with the help of the Euler rules [27].

As in the case of C_{60}, all leapfrogs can be considered to be truncations of the primitive fullerenes, in the sense that all the faces of the primitive have become isolated *islands*, surrounded by rings of hexagons. With every bond of the primitive is associated a perpendicular bond, which always forms a *bridge* between these islands. Based on this neat bond separation, two canonical valence-bond frames can be constructed for the leapfrog, which in a sense are the extremes of a correlation diagram, with the actual bonding somewhere in between. These bond schemes are known as the Fries and the Clar structures. The Fries structure is an extreme case where all *bridges* are isolated π-bonds. The induced representation for these bonds corresponds to $\Gamma_\sigma(e^P)$. On the other hand, in the Clar structures the bonding is completely redistributed to aromatic sextets on the hexagonal and pentagonal islands. The corresponding representation is the fibre bundle $\Gamma_\sigma(f^P) \times \Gamma_T$. We now compare the representations of both bonding schemes, using the symmetry theorems. We start with the main theorem, applied to the primitive P, and multiply left and right with Γ_R.

$$\Gamma_\sigma\left(v^P\right) \times \Gamma_R - \Gamma_\parallel\left(e^P\right) \times \Gamma_R + \Gamma_\circlearrowleft\left(f^P\right) \times \Gamma_R = \Gamma_T + \Gamma_R \tag{6.144}$$

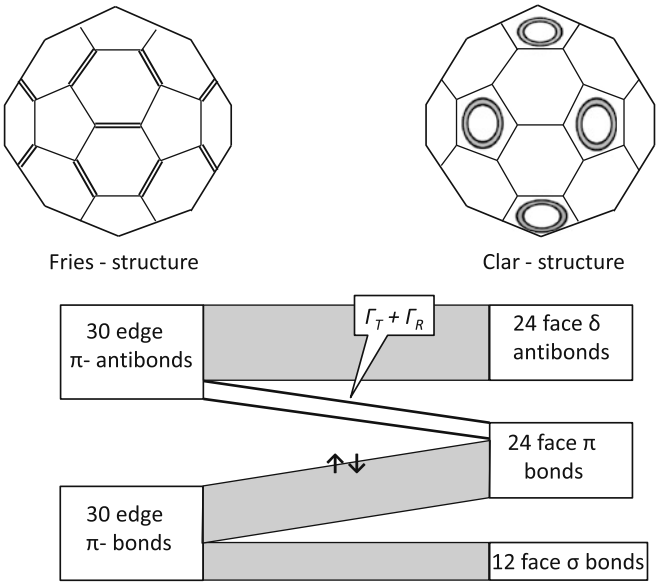

Fig. 6.11 Correlation diagram for C_{60}. The Fries and Clar structures are bonding extremes, where double bonds are either localized on the 30 bonds between the pentagons (Fries), or form isolated aromatic sextets on the twelve pentagons. The true conjugation scheme is found in between, and is characterized by six unoccupied levels, which are anti-bonding in the Fries structure and bonding in the Clar structure, and which transform as rotations and translations. Buckminsterfullerene has low-lying LUMO and LUMO+1 levels of $t_{1u}(\Gamma_T)$ and $t_{1g}(\Gamma_R)$ symmetry

Since $\Gamma_R = \Gamma_T \times \Gamma_\epsilon$, we could already simplify the face term to a form which precisely corresponds to the Clar representation:

$$\Gamma_{\circlearrowleft}\left(f^P\right) \times \Gamma_R = \Gamma_\sigma\left(f^P\right) \times \Gamma_T = \Gamma_{\text{Clar}} \tag{6.145}$$

The vertex term can be expressed with the help of Eq. (6.141):

$$\text{Trivalent:} \quad \Gamma_\sigma\left(v^P\right) \times \Gamma_R = \Gamma_\sigma\left(e^P\right) \times \Gamma_\epsilon + \Gamma_\parallel\left(e^P\right) \times \Gamma_\epsilon = \Gamma_{\circlearrowleft}\left(e^P\right) + \Gamma_\perp\left(e^P\right) \tag{6.146}$$

where the pseudo-scalar irrep turns a σ-object into a circular current, and rotates the parallel edge current over 90°. Note that this is applied in the primitive cage, to the edges of P only. To complete the derivation one final fibre bundle is needed, which applies to all convex polyhedra:

$$\Gamma_\sigma(e) \times \Gamma_T = \Gamma_\sigma(e) + \Gamma_\parallel(e) + \Gamma_\perp(e) \tag{6.147}$$

This result is based on the C_{2v} site-symmetry of an edge. The translation in this site has a radial σ-component of a_1 symmetry, and two tangential π-components of $b_1 + b_2$ symmetry. The fibre bundle will thus correspond to the induction of

$a_1 + b_1 + b_2$, which is precisely the meaning of the three terms on the right-hand side of Eq. (6.147). This expression may be transformed in two steps to the term which is required in the derivation. One first changes the substrate of the fibre from $\Gamma_\sigma(e)$ to $\Gamma_\parallel(e)$. This associates the edges with b_1 objects, and combination with $a_1 + b_1 + b_2$ will thus yield $b_1 + a_1 + a_2$, or:

$$\Gamma_\parallel(e) \times \Gamma_T = \Gamma_\parallel(e) + \Gamma_\sigma(e) + \Gamma_\circlearrowleft(e) \tag{6.148}$$

Finally, multiply this result by Γ_ϵ:

$$\Gamma_\parallel(e) \times \Gamma_R = \Gamma_\perp(e) + \Gamma_\circlearrowleft(e) + \Gamma_\sigma(e) \tag{6.149}$$

We now combine Eqs. (6.146) and (6.149), and find:

$$\text{Trivalent:} \quad \Gamma_\parallel\left(e^P\right) \times \Gamma_R - \Gamma_\sigma\left(v^P\right) \times \Gamma_R = \Gamma_\sigma\left(e^P\right) = \Gamma_{\text{Fries}} \tag{6.150}$$

This is precisely the representation of the Fries bonds. We can thus compare the Fries and Clar structures in a general leapfrog, and find from Eq. (6.144):

$$\Gamma_{\text{Clar}} - \Gamma_{\text{Fries}} = \Gamma_T + \Gamma_R \tag{6.151}$$

The Clar structure thus has six extra bonding orbitals as compared with the Fries structure. When both bonding schemes are correlated, as illustrated in Fig. 6.11, this sextet must correlate with the anti-bonding half of the Fries structure. It will thus be placed on top of the Clar band, and actually be nearly non-bonding, forming six low-lying virtual orbitals, which explains the electron deficiency of the leapfrog fullerenes. Moreover, as the derivation shows, they transform exactly as rotations and translations.

6.11 Problems

6.1 A three-electron wavefunction in an octahedron is given by:

$$\Psi = \left|(t_{1u}x\alpha)(t_{1u}y\alpha)(t_{1u}z\alpha)\right| \tag{6.152}$$

The vertical bars denote a Slater determinant. Determine the symmetry of this function, starting from parent two-electron coupled states, to which the third electron is coupled. Make use of the coupling coefficients in Appendix F.

6.2 Write the Jahn-Teller matrix for a threefold degenerate T_{1u} level in an icosahedral molecule. How many reduced matrix elements are needed?

6.3 Do you expect octahedral e_g orbitals to show a magnetic dipole moment?

6.4 Binaphthyl consists of two linked naphthalene molecules. The dihedral angle between the two naphthyl planes is around 70°, and can be stabilized by bulky substituents on the naphthyl units, as indicated below for the case of 2, 2′-diphenylphosphine-1, 1′-binaphthyl. A circular dichroism signal is detected in

the UV region, corresponding to the long-axis polarized transitions of the naphthyl units (indicated by the arrows in the figure). Construct the appropriate exciton states and determine the CD profile of the two enantiomers of binaphthyl.

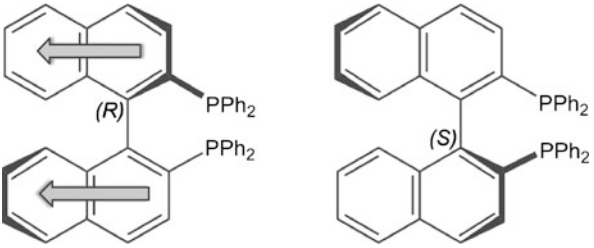

6.5 A diradical is a molecule with two *open* orbitals, each containing one electron. Consider as an example twisted ethylene (D_{2d} symmetry, see Fig. 3.9). The HOMO is a degenerate e-orbital, occupied by two electrons. Construct the e^2 diradical states for this molecule, and determine their symmetries.

6.6 Planar trimethylenemethane (TMM), C_4H_6, is a diradical with trigonal symmetry. Determine the Hückel spectrum for the four carbon p_z-orbitals perpendicular to the plane of the molecule. The HOMO in D_{3h} has e'' symmetry and is also occupied by two electrons. Determine the corresponding diradical states, and compare with the results for twisted ethylene. How would you describe the valence bond structure of this molecule?

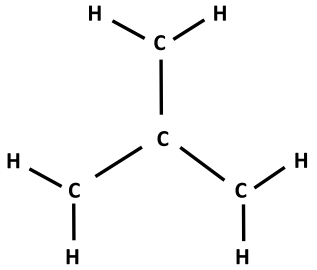

References

1. Wigner, E.P.: Group Theory. Academic Press, New York (1959)
2. Griffith, J.S.: The Irreducible Tensor Method for Molecular Symmetry Groups. Prentice Hall, Englewood-Cliffs (1962)
3. Butler, P.H.: Point Group Symmetry Applications, Methods and Tables. Plenum Press, New York (1981)
4. Ceulemans, A., Beyens, D.: Monomial representations of point-group symmetries. Phys. Rev. A **27**, 621 (1983)
5. Lijnen, E., Ceulemans, A.: The permutational symmetry of the icosahedral orbital quintuplet and its implication for vibronic interactions. Europhys. Lett. **80**, 67006 (2007)

6. Jahn, H.A., Teller, E.: Stability of polyatomic molecules in degenerate electronic states. I. Orbital degeneracy. Proc. R. Soc. A **161**, 220 (1937)
7. Bersuker, I.B.: The Jahn–Teller Effect. Cambridge University Press, Cambridge (2006)
8. Domcke, W., Yarkony, D.R., Köppel, H.: Conical Intersections, Electronic Structure, Dynamics and Spectroscopy. Advanced Series in Physical Chemistry, vol. 15. World Scientific, Singapore (2004)
9. Shapere, A., Wilczek, F.: Geometric Phases in Physics. Advanced Series in Mathematical Physics, vol. 5. World Scientific, Singapore (1989)
10. Judd, B.R.: The theory of the Jahn–Teller effect. In: Flint, C.D. (ed.) Vibronic Processes in Inorganic Chemistry. NATO Advanced Study Institutes Series, vol. C288, p. 79. Kluwer, Dordrecht (1988)
11. Bersuker, I.B., Balabanov, N.B., Pekker, D., Boggs, J.E.: Pseudo Jahn–Teller origin of instability of molecular high-symmetry configurations: novel numerical method and results. J. Chem. Phys. **117**, 10478 (2002)
12. Hoffmann, R., Woodward, R.B.: Orbital symmetry control of chemical reactions. Science **167**, 825 (1970)
13. Halevi, E.A.: Orbital symmetry and reaction mechanism, the OCAMS view. Springer, Berlin (1992)
14. Rodger, A., Nordén, B.: Circular Dichroism and Linear Dichroism. Oxford Chemistry Masters. Oxford University Press, Oxford (1997)
15. Orgel, L.E.: Double bonding in chelated metal complexes. J. Chem. Soc. 3683 (1961). doi:10.1039/JR9610003683
16. Ceulemans, A., Vanquickenborne, L.G.: On the charge-transfer spectra of iron(II)- and ruthenium(II)-tris(2, 2′-bipyridyl) complexes. J. Am. Chem. Soc. **103**, 2238 (1981)
17. Day, P., Sanders, N.: Spectra of complexes of conjugated ligands. 2. Charge-transfer in substituted phenantroline complexes: intensities. J. Chem. Soc. A **10**, 1536 (1967)
18. Yersin, H., Braun, D.: Localization in excited states of molecules. Application to $Ru(bipy)_3^{2+}$. Coord. Chem. Rev. **111**, 39 (1991)
19. Melvin, M.A.: Simplification in finding symmetry-adapted eigenfunctions. Rev. Mod. Phys. **28**, 18 (1956)
20. Ceulemans, A.: The construction of symmetric orbitals for molecular clusters. Mol. Phys. **54**, 161 (1985)
21. Biel, J., Chatterjee, R., Lulek, T.: Fiber structure of space of molecular-orbitals within LCAO method. J. Chem. Phys. **86**, 4531 (1987)
22. Ceulemans, A., Fowler, P.W.: Extension of Euler theorem to the symmetry properties of polyhedra. Nature **353**, 52 (1991)
23. Hilton, P.J., Wylie, S.: Homology Theory. Cambridge University Press, Cambridge (1967)
24. Hoffmann, R.: Building bridges between inorganic and organic chemistry (Nobel lecture). Angew. Chem., Int. Ed. Engl. **21**, 711 (1982)
25. Mingos, D.M.P., Wales, D.J.: Introduction to Cluster Chemistry. Prentice Hall, Englewood-Cliffs (1990)
26. Fowler, P.W., Manolopoulos, D.E.: An Atlas of Fullerenes. Clarendon, Oxford (1995)
27. Fowler, P.W., Ceulemans, A.: Electron deficiency of the fullerenes. J. Phys. Chem. A **99**, 508 (1995)